Alma Mater Studiorum Università di Bologna
Archivio istituzionale della ricerca

A constructal approach applied to the cooling of semi-elliptical blocks assembled into a rectangular channel under forced convection

(Article begins on next page)

16 January 2025

A CONSTRUCTAL APPROACH APPLIED TO THE COOLING OF SEMI-ELLIPTICAL BLOCKS ASSEMBLED INTO A RECTANGULAR CHANNEL UNDER FORCED CONVECTION

A. L. Razera[1], R.J.C. da Fonseca[1], L. A. Isoldi[2], E. D. dos Santos[2], L. A. O. Rocha[3], and C. Biserni[4]

[1]Department of Mechanical Engineering, Federal University of Rio Grande do Sul – UFRGS, Sarmento Leite Street, 425, Porto Alegre, RS, Brazil.

[2]Graduate Program of Ocean Engineering, School of Engineering, Federal University of Rio Grande – FURG, Rio Grande, Brazil, Italia Avenue, km 8, 96201-900.

[3]Mechanical Engineering Graduate Program, University of Vale do Rio dos Sinos – UNISINOS, São Leopoldo, RS, Brazil.

[4]Department of Industrial Engineering (DIN), Alma Mater Studiorum - University of Bologna, Bologna, Italy.

Abstract

This study investigates numerically the design of heated semi-elliptical blocks assembled inside of forced convective channel flows. The Constructal Design method, associated with the exhaustive search, was used to determine the restrictions, the degrees of freedom, the performance indicators, and the modality to sweep the search space of solutions. The degrees of freedom were defined as the ratios between the vertical and horizontal lengths of the semi-elliptical blocks, while the blocks and channel reference areas represented the constraints. The air flow ($Pr = 0.72$) is assumed as two-dimensional, incompressible, laminar, and steady-state. The fluid dynamic and thermal performances are evaluated for different Reynolds numbers (Re_H =10, 50, and 100). The multi-objective assessment of the problem was carried out using the Technique for Order Preference by Similarity to Ideal Solution method. Conservation equations of mass, momentum, and energy are solved numerically using the Finite Volume Method. The results indicated important gains on the thermal and fluid dynamic performances of nearly 76% and 1275%, respectively when the best and worst shapes were compared in the first optimization level. It is worth mentioning that, in the multi-objective viewpoint, the employed method above-cited correctly indicated the best configurations and the gain of performance in comparison with the pressure drop minimization and the heat transfer rate maximization.

Keywords: elliptical blocks, cooling, forced convection, numerical study, Constructal Design method

Nomenclature

A	Auxiliary area inside of the channel, m^2
A_f	Area of the block, m^2
A_s	Surface area of the block, m^2
g	Gravity acceleration, m/s^2
h	Heat transfer coefficient, W/m^2.K
$\bar{h}$	Average heat transfer coefficient, W/m^2.K
H	Height of the channel, m
H_1	Height of the block 1, m
H_2	Height of the block 2, m
k	Thermal conductivity, W/m.K
L	Distance between the block centers, m
L_u	Flow inlet length, m
L_d	Flow outlet length, m
L_1	Length of the block 1, m
L_2	Length of the block 2, m
Nu	Nusselt number
$\tilde{q}$	Dimensionless global heat transfer
$\tilde{q}_1$	Dimensionless global heat transfer on Block 1
$\tilde{q}_2$	Dimensionless global heat transfer on Block 2
P	Pressure, Pa
Re	Reynolds number
T	Temperature, K
u	Velocity in the x-direction, m/s
v	Velocity in the y-direction, m/s
x, y	Cartesian coordinates, m

Greek symbols

α	Thermal diffusivity, m²/s
ΔP	Pressure difference between domain Inlet and Outlet
μ	Dynamic viscosity, kg/m.s

υ	Kinematic viscosity, m^2/s
ρ	Density, kg/m^3
ϕ_1	Area fraction of the blocks in relation to the reference area of the channel
ϕ_2	Area fraction between blocks 1 and 2

Subscripts

F	Fluid dynamic analysis
G	Global
H	Based on channel height
max	Maximum
min	Minimum
T	Thermal analysis
TMO	TOPSIS multi-objective
W	Wall
ws	Worst performance geometry
1	Block 1
1o	Once optimized geometry
2	Block 2
2o	Twice optimized geometry
∞	Free flow

Superscripts

| (˜) | dimensionless variables |
| (ˉ) | spatial-averaged variables |

1. INTRODUCTION

The study of flows with heat transfer in vertical and horizontal channels containing heated obstacles inside has been the subject of several and exhaustive researches over the years. These convective flows ideally represent thermal systems often found in the engineering field and constitute a fundamental study in the cooling of electronic packages. A particularity of this type of system is the need for efficient performance in heat dissipation since its failure rates are directly related to the maximum temperature allowed in its components [1,2]. This theme presents

3

fundamental importance in the current scenario since technological advances have led to the miniaturization of electronic devices, resulting in more significant heat generation per unit volume of the components. Thus, there is a need to improve thermal equipment efficiency [3]. The application of this system model also expands to other essential areas in engineering, such as heat exchangers (solar air heaters, space heating systems, and domestic air conditioning), nuclear reactors, finned systems, among other thermal applications [4-11].

Flows in channels with heat-generating elements mounted inside them can be composed of different models of arrangements and geometries. These blocks can act only as a heat-generating element (heat sources) without obstructing the flow or even work as an extended heated surface inside. Many ideas emerged from these studies, such as the geometric composition relevance of the systems in obtaining a more significant heat transfer between the fluid and the heated elements [12-21].

In this context, it has been demonstrated that designs based on the elliptical concept can improve thermal performance compared to other geometries. This fact was observed by Brauer [22] and Rocha et al. [23] in studies that compared the thermal performance of elliptical cylinder arrangements to circular cylinder arrangements in transverse flows. Similarly, Razera et al. [24] obtained a positive outcome when evaluating the thermal behavior of semi-elliptical fins compared to triangular and rectangular ones inserted in lid-driven convective cavity flows. Thus, the need for studies related to heated elliptical fins or blocks subjected to convective flows becomes evident since this type of system's thermal and fluid dynamic behaviors are significantly affected by its geometric characteristics. In addition, the geometric investigation for different operating conditions is essential to guide the initial stages of equipment projects and define their designs. Thus, the studies related to convective flows around elliptical bodies have been developed continuously over time [25-37].

In recent years, the Constructal Design method has established itself as a promising technique to investigate the design of any finite-size flow system, including thermal systems. This field initiated with the definition of the Constructal Theory, which is a mental viewing that the design of flow systems and its rhythm is a universal phenomenon and that it can be interpreted as the tendency of systems to flow in paths of less resistance [38,39]. The physical principle of generation and prediction of design and rhythm in flow systems is called the Constructal Law, which states, "*for any flow system of finite dimensions to persist in time, its geometry must evolve to provide greater access to its internal currents*" [40-42]. In engineering projects, the Constructal Design method has been successfully employed to define the performance indicators, restrictions,

and degrees of freedom of the systems, giving them the freedom to modify their geometry, aiming to obtain a geometric configuration that better distributes its imperfections [39, 43, 44].

The Constructal Design method has been successfully used to rationalize the geometric configuration in idealized systems applicable to various engineering equipment. Some examples of applications are flows over cylinder arrangements [45-49], flows in channels [50,51], conductive paths, arrays of fins and cavities [52-59], heat sinks [60,61], cavities with heated elements inside [62-64], solar energy [65], wave energy [66,67], heat transfer in non-Newtonian fluid flows over cylinders [31,68], among other areas.

For the multi-objective evaluation of the system, the TOPSIS (Technique for Order Preference by Similarity to Ideal Solution) method was applied, based on the concept that the optimum multi-objective solution of the system must present the shortest Euclidean distance from the positive ideal solution and at the same time be the furthest from the negative ideal solution. This method can be used in multi-purpose systems, where it is necessary to maximize one parameter – in this case, the dimensionless heat transfer between the blocks and the fluid flow – and to minimize another – in this situation, the pressure drop inside the channel [69]. This multi-criteria assessment technique has been used successfully in several applications in the context of thermal and fluid dynamics engineering [70-72].

Thus, the present work aims to evaluate the thermal and fluid dynamic behaviors regarding an arrangement that combines a rectangular channel with heated semi-elliptical elements inserted into its interior. The system is subjected to a laminar flow with the forced heat convection mechanism acting. For all geometric configurations, different velocity impositions within the channel were simulated, which are defined by the Reynolds number ($Re_H = 10$, $Re_H = 50$ and $Re_H = 100$). The Prandtl number (Pr) was fixed for all simulations, equal to 0.72. The Constructal Design method, associated with the Exhaustive Search, defines the geometries and evaluates the geometric variation effect over the system response. The degrees of freedom of the system are the ratios between the vertical and horizontal lengths of the semi-elliptical blocks. The Exhaustive Search method needs a huge effort in obtaining the optimal result. However, it allows a wide view of the system's performance as its geometric configuration is modified, ensuring that the best solution is found. The numerical solution of the equations of conservation of mass, linear momentum, and energy was obtained based on the finite volume method through the commercial code of computational fluid dynamics FLUENT® [73-75]. In this context, the geometric rationalization obtained through the Constructal Design application provides a complete visualization of the problem's thermal and fluid dynamic behaviors, making it possible to propose solutions that can be extrapolated to actual operating conditions. For instance, the theoretical recommendations obtained

5

here can support the future design of the arrangement of electronic packaging and elemental channels of micro-channel heat exchangers.

2. MATHEMATICAL MODELING

This study adopted the assumptions of the steady-state regime, incompressible fluid and laminar forced convective flows with constant thermophysical properties. Thus, the equations of continuity, the balance of linear momentum (in the x and y directions), and energy, solved numerically here, are given, respectively, by [76]:

$$\frac{\partial u}{\partial x} + \frac{\partial v}{\partial y} = 0 \tag{1}$$

$$\rho\left(u\frac{\partial u}{\partial x} + v\frac{\partial u}{\partial y}\right) + \frac{\partial P}{\partial x} - \mu\left(\frac{\partial^2 u}{\partial x^2} + \frac{\partial^2 u}{\partial y^2}\right) = 0 \tag{2}$$

$$\rho\left(u\frac{\partial v}{\partial x} + v\frac{\partial v}{\partial y}\right) + \frac{\partial P}{\partial y} - \mu\left(\frac{\partial^2 v}{\partial x^2} + \frac{\partial^2 v}{\partial y^2}\right) = 0 \tag{3}$$

$$\rho C_p\left(u\frac{\partial T}{\partial x} + v\frac{\partial T}{\partial y}\right) - k\left(\frac{\partial^2 T}{\partial x^2} + \frac{\partial^2 T}{\partial y^2}\right) = 0 \, , \tag{4}$$

where x and y are the Cartesian coordinates in the horizontal and vertical directions, u and v are the velocities in horizontal and vertical directions of the flow, respectively, P is the pressure, T is the temperature, ρ is the fluid density, μ is the dynamic viscosity, k is the thermal conductivity, and C_p is the specific heat.

In order to generalize the results, the problem parameters can be used in their dimensionless form, such as:

$$\left(\tilde{x}, \tilde{y}, \tilde{H}, \tilde{L}, \tilde{H}_1, \tilde{H}_2, \tilde{L}_1, \tilde{L}_2\right) = \frac{\left(x, y, H, L, H_1, H_2, L_1, L_2\right)}{H} \tag{5}$$

$$\left(\tilde{u}, \tilde{v}\right) = \frac{\left(u, v\right)}{u_{in}} \tag{6}$$

$$\tilde{T} = \frac{T - T_\infty}{T_w - T_\infty} \quad (7)$$

$$\tilde{P} = \frac{\Delta P}{\rho(u_{in(Re_H=100)}^2)} \,, \quad (8)$$

where H is the channel height, u_{in} is the velocity at the channel inlet, T_w is the temperature in the blocks walls, T_∞ is the temperature at the channel's inlet, and ΔP is the pressure drop along the channel.

The general objective of the work is to find the geometric configurations that lead to the maximization of the heat transfer rate between the heated blocks and the surrounding fluid, which is at a lower temperature. Configurations that offer less resistance to flow inside the channel are also sought. The proposed system is defined through Fig. 1, where it is possible to observe the boundary conditions assumed in this analysis. The blocks of semi-elliptical geometry are inserted in the lower wall of the horizontal channel. The impermeability and non-slip boundary conditions are applied on the upper and lower walls of the domain and blocks surfaces ($\tilde{u} = \tilde{v} = 0$). At the entrance to the domain, the flow is governed by the prescribed velocity condition, which is defined by the Reynolds number, while at the outflow, the condition of the fluid outlet region (outflow) is applied, where the velocity gradient, normal to the output boundary, is considered to be null ($\partial \tilde{u}/\partial \tilde{n}$ = 0). It is worth mentioning that the flow is caused by the imposition of the momentum at the channel inlet.

Regarding the thermal conditions, at the entrance of the channel, a constant temperature of low magnitude, $\tilde{T}_\infty = 0$, is adopted, while a higher temperature magnitude is imposed on the surface of the blocks, $\tilde{T}_W = 1$. In addition, the upper and lower walls of the channel have adiabatic conditions $(\partial \tilde{T}/\partial \tilde{x} = \partial \tilde{T}/\partial \tilde{y} = 0)$. The fluid and flow properties defined for the set of simulations are shown in Table 1.

Table 1 – Properties of the fluid and the flow

Property	Symbol	Magnitude	Unit

Prandtl number	Pr	0.720	dimensionless
Thermal conductivity	k	0.026	W/m.K
Dynamic viscosity	μ	1.860×10^{-5}	kg/m.s
Specific heat at constant pressure	C_p	1006	J/kg.K
Density	ρ	1.165	kg/m³
Thermal diffusivity	α	2.2184×10^{-5}	m²/s

The parameter used to quantify the thermal performance of the system is the heat transfer rate [76], determined through the following equation:

$$q_{1,2} = \overline{h}_{1,2} \cdot A_{s1,s2} \cdot \left(T_w - T_\infty\right) \tag{9}$$

in which $q_{1,2}$ is the heat transfer rate on the surface of the block, $\overline{h}_{1,2}$ is the average heat transfer coefficient on the block, (T_w - T_∞) is the temperature difference between the block wall and the fluid, and $A_{s1,s2}$ are the surface areas of contact between the blocks and the fluid. Thus, from Eq. (9), the dimensionless group that is adopted to assess the effects of heat transfer by forced convection on the system can be defined as follows:

$$\tilde{q}_{1,2} = \frac{q_{1,2}}{k \cdot H \cdot \left(T_{Max} - T_{Min}\right)} \tag{10}$$

where (T_{Max} − T_{min}) is the maximum temperature difference in the system. Thus, the total dimensionless heat transfer within the system is determined by

$$\tilde{q} = \frac{q_1}{k \cdot H \cdot \left(T_{Max} - T_{Min}\right)} + \frac{q_2}{k \cdot H \cdot \left(T_{Max} - T_{Min}\right)} \tag{11}$$

In order to evaluate the thermal effect related to the heat transfer coefficient on the heated bodies surface, the Nusselt number was introduced as the ratio between convection and conduction heat transfer [76], in other words, the magnitude of heat transfer between the heated surface and the fluid:

$$Nu_H = \frac{h \cdot H}{k} = \frac{\partial \tilde{T}}{\partial \tilde{n}} \tag{12}$$

in which, h is the heat transfer coefficient, H is the characteristic length of the flow, and n is the normal coordinate of the surface of the blocks.

The Reynolds number (Re_H), which describes the flow regime, is defined by [77]:

$$Re_H = \frac{\rho \cdot u_{in} \cdot H}{\mu} \tag{13}$$

where Re_H is calculated considering the height of the channel (H) as the characteristic length.

For the geometric analysis, the Constructal Design method associated with the Exhaustive Search was used to determine the restrictions, the degrees of freedom, and the performance indicators in the geometric evaluation of the system. Thus, the problem is addressed with the two semi-elliptical blocks inserted in the lower wall of the channel, and the system has two geometric restrictions. The first one is determined through the auxiliary area (A) defined inside the channel, which represents a multiplication between the height of the channel (H) and the distance between the centers of the heated elements (L), given according to:

$$A = H \cdot L \tag{14}$$

The second one is given by the areas of the blocks inserted inside the channel:

$$A_{f1, f2} = \frac{\pi \cdot H_{1,2} \cdot L_{1,2}}{4} \tag{15}$$

Accordingly, two dimensionless relations for the system are defined: ϕ_1 and ϕ_2. The ratio ϕ_1 is the area fraction that blocks occupy within the channel defined as:

$$\phi_1 = \frac{A_{f1} + A_{f2}}{A} \tag{16}$$

The area fraction ϕ_2 represents the proportion that the areas of the semi-elliptical blocks have among themselves and is given by:

$$\phi_2 = \frac{A_{f1}}{A_{f2}} \tag{17}$$

From this, the geometry of the system can be described for any value of ϕ_1 and ϕ_2.

The system evaluation process can be seen in Fig. 2, where a schematic representative of the optimization model through the exhaustive search is presented. Initially, the area fractions to be evaluated tend to be determined. Thus, ϕ_1 has its value fixed, i.e., $\phi_1 = 0.20$, which constitutes a channel in which the blocks occupy 20% of the area of the reference system. Moreover, the value of ϕ_2 was set at 1.00, which indicates that the semi-elliptical elements have the same area. The degrees of freedom were defined by the ratio between the height of the channel and the distance between the centers of the blocks (H/L), and the ratios between the vertical and horizontal lengths of the semi-elliptical elements (H_1/L_1 and H_2/L_2). For this study, the ratio H/L is kept constant and equal to the unit ($H/L = 1$); therefore, the distance between the centers of the blocks is equal to the height of the channel ($L = H$). The aspect ratio H_2/L_2 is evaluated on the first optimization level while the ratio H_1/L_1 is kept fixed. Thus, the first level of system optimization is reached through the ratio of H_2/L_2, where the system is named as once optimized $(H_2/L_2)_{1o}$. At the second optimization level, the ratio H_2/L_2 is varied again for another fixed value of H_1/L_1, and this process is repeated for all ratios H_1/L_1. Hence, the ratio H_1/L_1 once optimized is obtained, $(H_1/L_1)_{1o}$, and the ratio H_2/L_2 reaches its second optimization level, $(H_2/L_2)_{2o}$. The degrees of freedom H_1/L_1 and H_2/L_2 are evaluated according to the following values: $0.1 \leq H_1/L_1, H_2/L_2 \leq 6.0$. In order to better represent the use of the Constructal Design method associated with the Exhaustive Search, its application is illustrated in Fig. 3, where a flowchart with the main stages of application of the method is presented [78].

The Technique for Order Preference by Similarity to Ideal Solution (TOPSIS) was employed to determine the multi-objective result of the problem. Its formulation is based on the concept that the optimal multi-objective solution of the system must present the shortest Euclidean distance from the positive ideal solution and, at the same time, be the furthest from the negative ideal solution. The present work needs to maximize one performance indicator – the dimensionless heat transfer between the blocks and the fluid ($\tilde{q}$) – and minimize another – the pressure drop inside the channel (ΔP). In addition, it is possible to determine the weight of importance that each objective has for the system according to the project's needs through the TOPSIS method. This method is developed according to the following steps [69]:

- Step 1 – Create a matrix $(x_{i,j})_{m \times n}$ with m alternatives (range of geometries) and n objectives (system performance indicators).

- Step 2 – Build the normalized decision matrix $(r_{i,j})_{m \times n}$: this process transforms the dimensional parameters of the system ($\tilde{q}$ and ΔP) into dimensionless attributes, thus enabling a comparison between them. In this work, the normalization is applied through Eq. (18), where all values of $\tilde{q}$ and ΔP (matrix $(x_{i,j})_{m \times n}$) are converted into normalized quantities.

$$r_{i,j} = \frac{x_{i,j}}{\sqrt{\sum_{i=1}^{m} x_{i,j}^2}} \rightarrow \frac{\tilde{q}_{i,j}}{\sqrt{\sum_{i=1}^{m} \tilde{q}_{i,j}^2}} \text{ and } \frac{\Delta \tilde{P}_{i,j}}{\sqrt{\sum_{i=1}^{m} \Delta \tilde{P}_{i,j}^2}} \tag{18}$$

- Step 3 – Build the weighted normalized decision matrix $(V_{i,j})_{m \times n}$: in this step, a set of weights is assigned to the normalized decision matrix $((r_{i,j})_{m \times n})$. In this way, each normalized attribute is multiplied by its associated weight, and the sum of the weights for the attributes must be equal to unity, according to Eqs. (19) and (20).

$$w = (w_1, w_2, ..., w_j, ..., w_n), \sum_{j=1}^{n} w_j = 1 \tag{19}$$

$$V_{i,j} = r_{i,j} \cdot w_j \tag{20}$$

In the case of this paper, w_1 is the weight associated with thermal relevance, and w_2 is the weight associated with fluid dynamic relevance.

- Step 4 – Classification of the benefit and non-benefit parameters of the system: In this study, the benefit parameter is the dimensionless heat transfer rate ($\tilde{q}$) (performance indicator to be maximized, i.e., greater is better), and the non-benefit parameter is the pressure drop inside the channel (ΔP) (performance indicator to be minimized, i.e., smaller is better).

- Step 5 – Definition of the positive ideal (V^+) and negative ideal (V^-) artificial solutions for the system. In thermal evaluation, the dimensionless heat transfer rate is a benefit parameter, so the positive ideal artificial solution contemplates the maximum weighted normalized

11

value of $\tilde{q}$. In fluid dynamic analysis, the purpose is to minimize the pressure drop inside the channel; thus, the positive ideal artificial solution will contemplate the lowest weighted normalized value of ΔP. In this sense, the ideal artificial solution for the system is obtained by Eq. (21). On the other hand, the negative ideal artificial solution of the system is defined by the smallest weighted normalized value of $\tilde{q}$ along with the largest weighted normalized value of ΔP, i.e., the worst possible artificial solution for the problem, obtained through Eq. (22).

$$V^+ = \left\{ \left(\max_i V_{i,j} \,\middle|\, j \varepsilon J \right), \left(\min_i V_{i,j} \,\middle|\, j \varepsilon J' \right) \,\middle|\, i = 1, 2, ..., m \right\} \to (\tilde{q}^+; \Delta \tilde{P}^+) \tag{21}$$

$$V^- = \left\{ \left(\min_i V_{i,j} \,\middle|\, j \varepsilon J \right), \left(\max_i V_{i,j} \,\middle|\, j \varepsilon J' \right) \,\middle|\, i = 1, 2, ..., m \right\} \to (\tilde{q}^-; \Delta \tilde{P}^-) \tag{22}$$

In Eqs. (21) and (22), J is associated with the benefit criterion, and J' is associated with the cost criterion.

- Step 6 – Calculation of the Euclidean distance of each alternative (geometric set) in relation to the positive and negative ideal artificial solutions: the distance between each alternative can be measured by the dimensionless Euclidean distance, representing the relative distance of each weighted normalized value in relation to the positive ideal artificial solution and the negative ideal artificial solution, being calculated, respectively, by:

$$S_i^+ = \sqrt{\sum_{j=1}^{m} (V_{i,j} - V_j^+)^2} \to Ex : S_1^+ = \sqrt{(\tilde{q}_{1,1} - \tilde{q}^+)^2 + (\Delta \tilde{P}_{1,2} - \Delta \tilde{P}^+)^2} \tag{23}$$

$$S_i^- = \sqrt{\sum_{j=1}^{m} (V_{i,j} - V_j^-)^2} \to Ex : S_1^- = \sqrt{(\tilde{q}_{1,1} - \tilde{q}^-)^2 + (\Delta \tilde{P}_{1,2} - \Delta \tilde{P}^-)^2} \tag{24}$$

- Step 7 – Calculate the multi-objective performance indicator in relation to the ideal solution (C_i): the score of the geometries evaluated based on the positive and the negative ideal solutions is determined as

$$C_i = \frac{S_i^-}{(S_i^+ + S_i^-)}, 0 < C_i < 1 \tag{25}$$

in which the solutions with the highest values of Ci are closer to the positive ideal solution and more distant from the negative ideal solution within the range $0 > C_i > 1$.

3. NUMERICAL MODELING

For the simulation of the laminar flows with heat transfer under forced convection, the conservation equations of mass, linear momentum, and energy were solved using the commercial code for fluid dynamics ANSYS FLUENT 14.0, based on the finite volume method [73-75]. For all simulated configurations, the spatial discretization was built through quadrilateral volumes. Regarding the treatment of advective terms, the interpolation scheme adopted was the Second-Order Upwind in the momentum and energy equations solution and the scheme named "PRESTO!" for the pressure discretization. The pressure-speed coupling was solved using the SIMPLE method. The number of volumes adopted for the system mesh was determined using successive refinements, increasing the number of volumes approximately twice (or more) with each refinement to establish a number of volumes that does not influence the study results. Thus, the results are considered independent of the mesh when the relative deviation of the dimensionless heat transfer between meshes of different numbers of volumes is less than 0.2%.

Table 2 shows the results regarding mesh quality for flows under the effect of forced convection, considering $Re = 100$ and $Pr = 0.72$, as well as the following geometric configuration: $\phi_1 = 0.2$; $\phi_2 = 1.0$; $H/L = 1.00$; $H_1/L_1 = 3.00$; $H_2/L_2 = 3.00$; $\tilde{L}_u = 15$ and $\tilde{L}_d = 20$. The relative percentage deviation between the results is calculated as indicated in the equations described in Table 2, in which the indexes (j) and ($j+1$) represent the results of $\tilde{q}$ for the mesh to be evaluated and the next one with the largest number of volumes, respectively. The lengths of the domain's inlet (L_u) and outlet (L_d) were evaluated not to generate interference in the numerically simulated results. Therefore, it was found that the mesh is considered suitable for the present study when it has approximately 50,000 volumes since the deviations presented between the successive results were less than 0.2%

Table 2 – Study of mesh quality for the forced convection flow

N. of Volumes	$\widetilde{q}_1$	$100 \cdot \dfrac{\left\|\tilde{q}_{1,(j)} - \tilde{q}_{1,(j+1)}\right\|}{\tilde{q}_{1,(j)}}$	$\widetilde{q}_2$	$100 \cdot \dfrac{\left\|\tilde{q}_{2,(j)} - \tilde{q}_{2,(j+1)}\right\|}{\tilde{q}_{2,(j)}}$	$\tilde{q}$	$100 \cdot \dfrac{\left\|\tilde{q}_{(j)} - \tilde{q}_{(j+1)}\right\|}{\tilde{q}_{(j)}}$
3,228	7.4573	3.6559	5.5620	1.4554	13.0194	2.7158
12,654	7.1847	0.1666	5.4811	0.3212	12.6658	0.0445
50,945	**7.1727**	**0.0107**	**5.4987**	**0.0954**	**12.6714**	**0.0353**
108,047	7.1720	0.1151	5.5039	0.0276	12.6759	0.0771
202,716	7.1637	---	5.5024	---	12.6661	---

Once the numerical and mathematical models are established, a verification of the adopted methodology is also required.

Thus, it was sought to reproduce flow systems with thermal and fluid dynamic characteristics similar to those of the present work, favoring a quantitative comparison between the results. Hence, for the verification of the numerical and mathematical models of forced convection flow, the empirical correlations of Churchill and Bernstein [79] and Hilpert [80], which define the average Nusselt number for the effect of forced convection on circular cylinders in free flow, were used. Furthermore, the model of this study was also verified through the correlation of Khan et al. [79], which defines the average Nusselt number for the effect of forced convection on a circular cylinder inserted in a channel between parallel plates.

This correlation is suitable for flows with $Re_d \geq 100$ and $Pr \geq 0.72$. The correlations of Churchill and Bernstein [79], Hilpert [80], and Khan et al. [81] are given, respectively, by:

$$\overline{Nu_d} = 0.3 + \frac{0.62 \cdot Re_d^{1/2} \cdot Pr^{1/3}}{\left[1 + \left(\dfrac{0.4}{Pr}\right)^{2/3}\right]^{1/4}} + \left[1 + \left(\frac{Re_d}{282000}\right)^{5/8}\right]^{4/5} \tag{26}$$

$$\overline{Nu_d} = C \cdot Re_d^m \cdot Pr^{1/3} \tag{27}$$

$$\overline{Nu_d} = \left[0.843 - 0.25 \cdot exp\left(-2.65 b^{2.5}\right)\right] Re_d^{1/2} Pr^{1/2} \tag{28}$$

where $\overline{Nu_d}$ is the average Nusselt number calculated around the cylinder. The variables *C* and *m* in Eq. (27) are determined using the Reynolds number (Re_d) of the flow and can be obtained from Hilpert [80] and Incropera et al. [82]. In Eq. (28), the variable *b* represents the blocking ratio of the cylinder within the channel (d/S_t), calculated as the ratio between the diameter of the cylinder (*d*) and the distance between the plates (S_t) [81].

Consequently, when the heat transfer was evaluated in a cylinder inserted between two parallel flat plates, as shown in Table 3, it was found that the model is adequate for the solution of the problem since the deviation presented between the result of this work ($\overline{Nu_{d,N}}$) and that obtained through the correlation proposed by Khan et al. [81] ($\overline{Nu_{d,C}}$), was less than 3%. Furthermore, Table 4 shows that the numerical and mathematical models of this work – when applied in a system that evaluates a forced convective flow over a cylinder with no blockage, i.e., upper and lower plates far enough to avoid interference over the results in the cylinder – also showed quantitative conformity with results already consolidated in the literature, since, for all flow conditions applicable, the deviations between the solutions presented here ($\overline{Nu_{d,N}}$) and the empirical correlations of Hilpert [80] and Churchil and Bernstein [79] ($\overline{Nu_{d,C}}$) remained below 5% in practically all evaluations.

Table 3 – Verification of the numerical and mathematical models of the flow under the effect of forced convection through the correlation of Khan et al. [81].

Flow - $Re_d = 100$ and $Pr = 0.72$			
		$\overline{Nu_d}$	
Re_d $b(d/S_t)$	Present Study	Khan et al., 2004	$\dfrac{100 \cdot \left\lvert \overline{Nu_{d,N}} - \overline{Nu_{d,C}} \right\rvert}{\overline{Nu_{d,N}}}$
100 0.1	5.4571	5.3336	2.2632

Table 4 – Verification of the numerical and mathematical models of the flow under the effect of forced convection through the empirical correlations of Hilpert [80] and Churchil and Bernstein [79].

	$\overline{Nu_d}$				
Re_d	Present Study	Hilpert, 1930	$100 \cdot \dfrac{\left| \overline{Nu_{d,N}} - \overline{Nu_{d,C}} \right|}{\overline{Nu_{d,N}}}$	Churchill and Bernstein, 1977	$100 \cdot \dfrac{\left| \overline{Nu_{d,N}} - \overline{Nu_{d,C}} \right|}{\overline{Nu_{d,N}}}$
10	1.9278	1.9814	2.7807	1.8465	4.2139
50	3.7135	3.6818	0.8532	3.7660	1.4139
100	5.1725	5.2344	1.1954	5.2113	0.7491

4. RESULTS AND DISCUSSIONS

The simulations determined the values of the aspect ratios H_1/L_1 and H_2/L_2 that lead to the maximization of the heat transfer rate through the blocks inside the channel and the minimization of the pressure difference between the regions of inlet and outlet of the channel. The aspect ratios H_1/L_1 and H_2/L_2 were evaluated in the range $0.10 \leq H_1/L_1$ and $H_2/L_2 \leq 6.0$. For all geometric configurations, different velocity impositions were simulated inside the channel, defined by the Reynolds number (in this paper, for the following values: $Re_H = 10$, $Re_H = 50$ and $Re_H = 100$). The Prandtl number was fixed for all simulations at the value $Pr = 0.72$. In total, 675 simulations were carried out, corresponding approximately to 130 h of processing.

The surfaces in Fig. 4 show the global behavior of the dimensionless heat transfer rate $\tilde{q}$ as a function of the degrees of freedom H_1/L_1 and H_2/L_2 for the different values of Re_H considered. In Fig. 4a, in which the flow with $Re_H = 10$ was studied, it is noticed that the geometric variation of the system – through the degrees of freedom H_1/L_1 and H_2/L_2 – did not significantly affect the dimensionless global heat transfer rate ($\tilde{q}$) between the blocks and the fluid, since the response surface obtained is similar to a horizontal plane, which does not have large amplitudes. On the other hand, in the evaluations performed on the flows defined by $Re_H = 50$ (Fig. 4b) and $Re_H = 100$ (Fig. 4c), one can observe a significant influence of the geometry of the blocks on the performance of the system. The response surfaces converge to points perceptible maximums, showing the existence of geometries that considerably favor the increase of the dimensionless global heat transfer rate in the system. In addition, according to Fig. 4, it is evident that the highest magnitudes of $\tilde{q}$ are obtained for flows with the highest numbers of Re_H studied.

Moreover, from Fig. 5, which shows the performance of the dimensionless heat transfer rate for each one of the blocks (block 1 ($\tilde{q}_1$) and block 2 ($\tilde{q}_2$)) as a function of the degrees of freedom

H_1/L_1 and H_2/L_2, it is possible to comprehend this behavior. When analyzing the thermal performance of the flow for $Re_H = 10$ (Fig. 5a), in which there is a lower imposition of momentum in the channel and the effects of heat diffusion through the environment are accentuated, the greater part of the total heat transfer of the system defines mainly on the surface of the block 1, since it is placed in the upstream region of the channel. It is also noticed that the individual performance of the blocks depends predominantly on the aspect ratio H_1/L_1, and the thermal performance of block 1 shows greater magnitudes of heat transfer compared to block 2. Besides, a seesaw effect can be observed in Fig. 5a in dimensionless heat transfer rates $\tilde{q}_1$ and $\tilde{q}_2$ since, with the augmentation of H_1/L_1, the dimensionless heat transfer of the block 1 ($\tilde{q}_1$) increases, while, with the increase of H_1/L_1, the dimensionless heat transfer on the surface of the block 2 ($\tilde{q}_2$) tends to decrease, which explains the horizontality of the global response of the system given by the response surface of Fig. 4a. It is also noteworthy (for the cases with $Re_H = 10$, i.e., Fig. 5a) that the variation in the degree of freedom H_2/L_2 has a little relevance in the thermal performance for both blocks, since, for the same value of H_1/L_1, the variation of H_2/L_2 does not cause a significant fluctuation in the dimensionless heat transfer rates $\tilde{q}_1$ and $\tilde{q}_2$.

Figs. 6 and 7 illustrate this effect more evidently; it is shown, respectively, the temperature fields for a selected set of geometries evaluated in the flow given by $Re_H = 10$ (Fig. 6) and the individual thermal performance of blocks 1 and 2 ($\overline{Nu_{H1,H2}}$, $\tilde{q}_{1,2}$, $A_{s1,s2}$) to visualize the thermal behavior of block 1, as a function of the geometric variation of the block 2 (H_2/L_2) – i.e., Fig. 7a –, and the thermal behavior of block 2, as a function of the geometric variation of block 1 (H_1/L_1) – Fig. 7b. Thus, for cases where the aspect ratio H_1/L_1 has a value less than or equal to the value of the aspect ratio H_2/L_2 (some cases are exemplified through Figs. 6a and 6b), a greater distributive balance between the gradients of temperature around blocks 1 and 2 is perceived, allowing the block 2, although positioned downstream in the system, to present higher heat transfer coefficients when compared to the configurations in which the values of H_1/L_1 are greater than H_2/L_2 (Figs. 6b and 6c). The curve of $\overline{Nu_{H2}}$, depicted in Fig. 7b, highlights this effect and presents that the heat transfer coefficients of block 2 (given by $\overline{Nu_{H2}}$) are also conditioned by the geometry of block 1, since, with the increase in the ratio H_1/L_1, or the same value of H_2/L_2, the heat transfer coefficient $\overline{Nu_{H2}}$ decreases drastically on the surface of block 2 (Fig. 7b). In this way, in these geometric configurations, block 2 comes into contact with the fluid at a higher temperature (Fig. 6c), and after that, the thermal gradients around it are reduced, and the heat transfer from block 2 to the fluid flow

is impaired. As well, through Fig. 7a, it can be observed that the variation of the aspect ratio H_2/L_2 does not influence the heat transfer of block 1, showing that, in this flow condition, the performance of the problem depends exclusively on the geometry of the block 1 because it is positioned upstream in the system.

Despite the importance of evaluating the effects of the average heat transfer coefficients on the surface of the blocks ($\overline{Nu_{H1}}$ and $\overline{Nu_{H2}}$), the dimensionless heat transfer rate ($\tilde{q}$) is strongly related to the surface area of heat transfer between the blocks and the surrounding flow. Thus, with the increase in the surface area of block 1 (A_{s1}) – mainly when this augmentation occurs transversely to the flow ($H_1/L_1 \geq 0.5$), there is a performance improvement of the dimensionless heat transfer rate since a greater surface area of the body comes into contact with the fluid at a lower temperature (Fig. 6c), leading to high heat transfer rates at the frontal region of the block 1. Thus, in Fig. 7a, it is observed that the gains related to the dimensionless heat transfer of the block 1 ($\tilde{q}_1$) are directly associated with the geometries that have the largest surface areas (A_{s1}), since the curves of $\tilde{q}_1$ and A_{s1} practically follow each other and, accordingly, a higher value of A_{s1} causes the blocks to dissipate a more significant amount of heat into the fluid, even in some cases where the average heat transfer coefficients ($\overline{Nu_{H1}}$) decreases.

Dissimilarity, in the case of block 2, which has its performance considerably affected by the geometry of block 1 (Fig. 7b), the increase in the surface area of the heated element (A_{s2}) is also a significant factor for obtaining better performance in relation to $\tilde{q}_2$. However, this performance is conditioned to the degree of freedom H_1/L_1 since it is block 1 that predominantly establishes the condition of the temperature gradients around block 2 in the system, conditioning its heat transfer coefficient $\overline{Nu_{H2}}$. Therefore, as observed in Fig. 7b, for the same surface area A_{s2}, the dimensionless heat transfer rate $\tilde{q}_2$ is drastically affected by the geometry of block 1.

It is also interesting to notice in Figs. 4b and 4c, in which the results for the global dimensionless heat transfer ($\tilde{q}$) are presented for flow conditions given by $Re_H = 50$ and $Re_H = 100$, respectively, a considerable influence of the evaluated degrees of freedom H_1/L_1 and H_2/L_2 in the thermal performance of the system. More precisely, the surfaces of heat transfer obtained converge to the point of maximum quite evident as the degrees of freedom H_1/L_1, and H_2/L_2 tend to their maximum values. In other words, when analyzing a fixed value of H_1/L_1, the curve that represents the variation of H_2/L_2 on the response surface reaches its maximum point for the highest value of H_2/L_2 studied; likewise, when considering a fixed value of H_2/L_2, the point of maximum performance is also obtained for the highest value of the evaluated ratio H_1/L_1. This behavior

becomes more evident as Re_H increases. In addition, through Figs. 5b and 5c, a more similar contribution of the blocks in the global dimensionless heat transfer of the system ($\tilde{q}$) is noticeable. Differently from the behavior obtained with $Re_H = 10$, block 2 presented, for several configurations, a thermal performance greater than or equivalent to the thermal performance of block 1 with the increase of Re_H.

This effect can be explained in Fig. 8, which shows the temperature fields for the geometries given by: (a) $H_1/L_1 = 0.4$, $H_2/L_2 = 0.4$; (b) $H_1/L_1 = 0.4$, $H_2/L_2 = 4.0$; and (c) $H_1/L_1 = 0.4$, $H_2/L_2 = 6.0$; for the different Reynolds numbers studied ($Re_H = 10$, $Re_H = 50$ and $Re_H = 100$). In Fig. 8a ($H_1/L_1 = 0.4$, $H_2/L_2 = 0.4$), it can be noticed that the increase in the Reynolds number causes a reduction in the thickness of the thermal boundary layer of the flow, providing that the temperature gradients around of block 2 are larger than the ones in block 1. The reduction in the thermal boundary layer thickness of the flow becomes even more beneficial for cases in which the ratio H_2/L_2 has a value greater than or equal to 4.0 ($H_2/L_2 \geq 4.0$), as shown in Figs. 8b and 8c: the heat transfer surface of block 2 expands transversely to the flow, making a portion of fluid at low temperature and favoring its thermal performance.

This behavior is even more evident in Fig. 9, which shows the effects of local heat transfer (Nu_{Local}) on the surfaces of blocks 1 and 2 in the geometric set given by $H_1/L_1 = 0.4$ and $H_2/L_2 = 6.0$ for: (a) $Re_H = 10$; (b) $Re_H = 50$ and (c) $Re_H = 100$ (the temperature fields for these same cases can be seen in Fig. 8c). As expected, the increase in the Reynolds number causes the convective heat transfer of the system to become accentuated. Thus, analyzing the same geometric configuration, a considerable performance increase in the local heat transfer coefficients of the blocks (Nu_{Local}) is observed, which occurs due to the appearance of high heat transfer spikes on their surfaces. These gains are more significant in block 2, which presents its geometry more elongated transversely in relation to the flow. In addition, the increase in the Reynolds number caused a flattening of the difference in thermal performance between the blocks, since the average heat transfer coefficients obtained on the surfaces of blocks 1 and 2 ($\overline{Nu_{H1}}$ and $\overline{Nu_{H2}}$) tend to have their values with more similar magnitudes, providing a greater heat transfer capacity of block 2 within the system. It is worth mentioning that this analysis is essentially valid for cases in which the degree of freedom H_2/L_2 has a value equal to or greater than 4.0 because, for these cases, the reduction in the thermal boundary layer thickness of the flow (with the increase of the Reynolds number) has a greater effect on the system, generating a considerable change in the thermal performance of block 2. Thus, for $Re_H = 10$ (Fig. 9a), the difference in performance between the heat transfer coefficients between blocks 1 and 2 was approximately 105% ($\overline{Nu_{H1}} = 3.3432$ and

$\overline{Nu_{H2}}$ = 1.6234). For Re_H = 50 (Fig. 9b), this difference decreased to approximately 40% ($\overline{Nu_{H1}}$ = 5.6678 and $\overline{Nu_{H2}}$ = 4.0231), while for Re_H = 100 (Fig. 9c), the performance difference between the heat transfer coefficients of the blocks was even lower, at around 29% ($\overline{Nu_{H1}}$ = 7.0638 and $\overline{Nu_{H2}}$ = 5.4643).

Another important aspect regarding the analysis of flows characterized by Re_H = 50 and Re_H = 100 (Figs. 4b, 4c, 5b and 5c) is the fact that, when the geometry H_2/L_2 is varied to a fixed value of H_1/L_1 (in this case, essentially for H_1/L_1 = 6.0) there is an episodic increase in the thermal performance of block 2 ($\tilde{q}_2$) for $H_2/L_2 \geq 1.0$, at Re_H = 100, and $H_2/L_2 \geq 0.9$, at Re_H = 50. This behavior is not seen for the other ratios H_1/L_1 (except for H_1/L_1 = 5.0 in the condition of Re_H = 100, where a slight deviation in behavior is observed in the same direction). Figure 10 is presented for better visualization: it can be seen, in isolation from the response surfaces of Figs. 4b and 4c, the curves related to dimensionless heat transfer, and depending on the variation in the degree of freedom H_2/L_2, considering H_1/L_1 = 6.0 fixed, for (a) Re_H = 50; and (b) Re_H = 100. The results demonstrate more evidence that this effect considerably affects the thermal performance of block 2 through $\tilde{q}_2$, which significantly influences the system's global dimensionless heat transfer rate of the system ($\tilde{q}$).

To deepen this mechanism, Fig. 11 is presented, considering Re_H = 100 for the geometries given by: (a) H_1/L_1 = 6.0 and H_2/L_2 = 0.9; (b) H_1/L_1 = 6.0 and H_2/L_2 = 1.0; (c) H_1/L_1 = 6.0 and H_2/L_2 = 4.0; and (d) H_1/L_1 = 6.0 and H_2/L_2 = 6.0. The topologies of Fig. 11a (H_1/L_1 = 6.0 and H_2/L_2 = 0.9) show that there is the formation of an intense flow between block 1 and the upper surface of the channel since it is imposed a momentum at the channel inlet. The flow downstream block 1 behaves similarly to that seen in a jet flow. This characteristic causes the flow reattachment on the lower surface of the domain downstream of block 2, resulting in block 2 being inserted in a region with low momentum intensity. Thus, block 2 practically does not interact with the main jet generated downstream of block 1, essentially with the fluid at a lower temperature.

Consequently, the mechanism of heat diffusion predominates between block 2 and the surrounding flow, reducing the heat transfer coefficients in this region. However, as H_2/L_2 increases its value up to 1.0 (Fig. 11b), the main flow downstream the block 1 starts to touch the surface of block 2, providing greater velocity fields in its surroundings. Moreover, the formation of a recirculation region between blocks 1 and 2 guarantees greater temperature gradients around the extended surfaces, being favorable to heat transfer. Figure 12 shows the effects of local heat transfer (Nu_Local) on the surfaces of blocks 1 and 2 for the same geometric set as in Fig. 11 and corroborates

the argumentations as mentioned earlier: it is evident (see Figs. 12a and 12b) the considerable increase in the local heat transfer coefficients around block 2 for the geometry of $H_2/L_2 = 1.0$ concerning $H_2/L_2 = 0.9$.

Regarding the geometries illustrated in Figs. 11c and 11d, in which there is a considerable increase in the height of block 2, a new flow restriction occurs. This restriction causes a recirculation zone in the middle of the heated blocks, which increases the temperature gradients between blocks 1 and 2, ensuring high heat transfer rates (Nu_{Local}) (Figs. 12c and 12d). In these geometric configurations, Figs. 12c ($H_1/L_1 = 6.0$ and $H_2/L_2 = 4.0$) and 12d ($H_1/L_1 = 6.0$ and $H_2/L_2 = 6.0$), although the average heat transfer coefficients over the blocks ($\overline{Nu_H}$) are slightly smaller compared to the set given in Fig. 12b ($H_1/L_1 = 6.0$ and $H_2/L_2 = 1.0$), the increase in the surface area of block 2 (A_{s2}) (due to the increase in the degree of freedom H_2/L_2) ensures that the high rates of the dimensionless heat transfer for block 2 are higher, and thus, more beneficial to the system in relation to the heat exchange, as it is visualized in Figs. 10a and 10b.

Coherently, Fig. 13 shows the sets of geometries of better performance $(H_2/L_2)_{T,1o}$ and their respective dimensionless heat transfer rates, $\tilde{q}$, $\tilde{q}_1$ and $\tilde{q}_2$ obtained in the first level of optimization, as a function of H_1/L_1 for: (a) $Re_H = 10$; (b) $Re_H = 50$; and (c) $Re_H = 100$. Thus, when evaluating different values of H_2/L_2 for fixed values of H_1/L_1, it was observed that the geometries of H_2/L_2 that reached the best thermal performances converged in the same result for the studied values of H_1/L_1 and Re_H, presenting as the optimal geometric point the ratio $(H_2/L_2)_{T,1o} = 6.0$. This effect shows that, by stretching block 2 across the flow, the best global thermal benefits of the system are achieved for all values of H_1/L_1 evaluated, corroborating the discussion of thermal phenomenology previously enunciated. Likewise, for the optimized geometries, it is noticed that for lower magnitudes of Reynolds (in this paper, $Re_H = 10$), the degree of contribution of each fin to the maximum heat transfer in the system is opposed to the extent that the degree of freedom H_1/L_1. Therefore, it increases this geometric change when combined with the greater diffusive effects of the system, causing element 2 to be surrounded by a layer of fluid at a higher temperature when compared to other geometric cases (Fig. 13a). On the other hand, for $Re_H = 50$ and $Re_H = 100$ (Figs. 13b and 13c), the optimal geometry of block 2 ($(H_2/L_2)_{T,1o} = 6.0$) maintains its performance practically insensitive to the variation of H_1/L_1.

Figure 14 shows the percentage difference in the performance of the cases once optimized ($(H_2/L_2)_{T,1o}$) in relation to the geometries that showed the lowest performance ($(H_2/L_2)_{T,ws}$) in the system within a first level optimization as a function of H_1/L_1, for: (a) $Re_H = 10$; (b) $Re_H = 50$; and (c) $Re_H = 100$. Initially, it can be highlighted that, for all the evaluated flow conditions, the

geometries with the lowest performance had their values less than 1 ($H_2/L_2 < 1.0$), evidencing once again the fact that the geometric elongation of block 2 in the horizontal flow direction proves to be unfavorable to the thermal performance of the system. Thus, in the first level of optimization, it is already possible to perceive the importance of the geometric evaluation of the set through the Constructal Design method, considering the great difference in performance between the optimum geometries and the cases of lower performance. For the cases evaluated by the flow given by $Re_H = 10$ (Fig. 14a), in which the performance differences between the geometries were smaller in relation to the other flow conditions studied, it is possible to notice a great increase in performance with reference to the optimized cases, obtaining improvements in the range from 12% to 31% in relation to the total dimensionless heat transfer rate within the system ($\tilde{q}$). For the cases under the conditions of $Re_H = 50$ and $Re_H = 100$ (Figs. 14b and 14c), the performance of the optimum geometries ((H_2/L_2)$_{T,1o}$) were even superior to the geometries of reduced performance ((H_2/L_2)$_{T,ws}$), showing gains in the thermal performance of the system in the range of 37% to 60% for $Re_H = 50$, and from 44% to 76% for $Re_H = 100$.

Focusing again on Fig. 13, but now evaluating the system at the second level of thermal optimization, where the aspect ratio H_1/L_1 is once optimized ((H_1/L_1)$_{T,1o}$) and the degree of freedom H_2/L_2 is twice optimized ((H_2/L_2)$_{T,2o}$), a relevant increase in performance is detected since the geometric configuration of the twice optimized system presented considerably superior results when compared to the optimal geometries in a first optimization level. Therefore, the importance of greater geometric freedom of the system to obtain better performance is evidenced. For $Re_H = 10$, the twice optimized geometry ((H_1/L_1)$_{T,1o} = 6.0$ and (H_2/L_2)$_{T,2o} = 6.0$) presented superior results on the dimensionless heat transfer rate ($\tilde{q}$), obtaining an increase in the approximate thermal performance of up to 13% in relation to the lowest optimum performance of the system obtained in the first level of optimization ($H_1/L_1 = 0.5$ and (H_2/L_2)$_{T,1o} = 6.0$). For the conditions of $Re_H = 50$ and $Re_H = 100$, this performance gain was even superior, where the approximate thermal gain of the twice optimized geometry ((H_1/L_1)$_{T,1o} = 6.0$ and (H_2/L_2)$_{T,2o} = 6.0$) was up to 33% for $Re_H = 50$ and 37% for $Re_H = 100$, when compared to lower performance geometries in a first optimization level ($H_1/L_1 = 0.6$ and (H_2/L_2)$_{T,1o} = 6.0$).

In a supplemental evaluation of Fig. 13, where a condition of maximum heat removal in the system is assumed, but with the need for equal heat removal between electronic devices (e.g., in an encapsulation system of electronic devices with equal cooling needs), the geometry that best provided this effect for the condition of $Re_H = 10$ is characterized by the coordinates $H_1/L_1 = 1.0$ and (H_2/L_2)$_{T,1o} = 6.0$ ($\tilde{q}_1 = 2.7555$; $\tilde{q}_2 = 2.8018$ and $\tilde{q} = 5.5574$), in which the difference in performance

between blocks 1 and 2 was less than 1.69% (see Fig. 13a). It is worth mentioning that this geometric configuration led to a decrease in the thermal performance of the system of approximately 12.78% in relation to the optimal global case obtained in the second level of optimization, where $(H_1/L_1)_{T,1o} = 6.0$ and $(H_2/L_2)_{T,2o} = 6.0$ ($\tilde{q}_1 = 4.6894$; $\tilde{q}_2 = 1.5781$ and $\tilde{q}_{max,2o} = 6.2676$), which showed a difference of performance between blocks 1 and 2 of approximately 197%, being block 1 dominant in the system in relation to the transfer rate of heat ($\tilde{q}$). For the flow condition given by $Re_H = 50$ and $Re_H = 100$, the geometric set that best provided this effect continued to be the twice optimized geometry (Figs. 13a and 13b), $(H_1/L_1)_{T,1o} = 6.0$ and $(H_2/L_2)_{T,2o} = 6.0$, where the performance difference between blocks 1 and 2 was less than 17.1% for $Re_H = 50$ and 13% for $Re_H = 100$.

In the fluid dynamic analysis of the problem, the main objective was to minimize the pressure difference between the entrance and the channel's exit, searching for a lower power requirement of the system, such as, for example, in relation to pumps or fluid blowers. Thus, Fig. 15 shows the fluid dynamic performance concerning the performance indicator ΔP, which is the representation of the pressure difference between the inlet and outlet of the flow, for (a) $Re_H = 10$; (b) $Re_H = 50$; and (c) $Re_H = 100$. Based on pure observations, the surfaces of Fig. 15 show that, for a fixed value of H_1/L_1, the behavior of the system as a function of the variation of H_2/L_2 is practically stable for values of H_2/L_2 less than or equal to 2 ($H_2/L_2 \leq 2.0$), demonstrating that the geometric variation of block 2 in the range $0.1 \leq H_2/L_2 \leq 2.0$ does not cause additional large pressure losses within the channel in the range of H_1/L_1 studied. However, as expected, for the geometries given by $H_2/L_2 > 2.0$, where block 2 starts to obstruct the flow more sharply, the worst fluid dynamic performances occur, which are accentuated as the value of H_2/L_2 tends to increase up to its maximum value of $H_2/L_2 = 6.0$. As an exception, in the results for $Re_H = 50$ ($H_1/L_1 = 6.0$) and $Re_H = 100$ ($H_1/L_1 = 6.0$, $H_1/L_1 = 5.0$ and $H_1/L_1 = 4.0$), an episodic decrease in pressure drop (ΔP) is observed inside the channel, which is accentuated with the increase of Re_H. This effect is similar to the phenomenon evaluated in Fig. 11, in which for these geometries, there is the formation of an intense flow between the blocks, where, in these geometric conditions, the flow starts a tangent to block 2, resulting in an increased heat transfer rate between the heated elements and the fluid, as previously seen. Now, under the fluid dynamics viewpoint, a decrease in pressure drop is perceived since it generates a better ability of the fluid to flow inside the channel, which benefits the system. In addition, through Fig. 15, specifically evaluating the degree of freedom H_1/L_1, the same effect is observed for H_2/L_2, given that the lower ratios of H_1/L_1 provide the lowest values of ΔP of the system, with stability pressure drop for values of H_1/L_1 less than or equal to 2 ($H_1/L_1 \leq 2.0$) and a

considerable loss of system performance for values of H_1/L_1 greater than two ($H_1/L_1 > 2.0$), due to greater flow obstruction caused by block 1, consequently raising the values of $\mathit{\Delta P}$ in the domain.

Figure 16 shows the sets of geometries of best $((H_2/L_2)_{F,1o})$ and worst $((H_2/L_2)_{F,ws})$ cases in relation to the fluid dynamic performance of the system obtained in a first level of optimization as a function of H_1/L_1 for: (a) $Re_H = 10$; (b) $Re_H = 50$; and (c) $Re_H = 100$. Fig. 17a, in which the flow with $Re_H = 10$ is evaluated, demonstrates that the values of H_2/L_2 that minimized the pressure difference inside the channel were practically constant for the different studied values of H_1/L_1, being represented by the lowest ratios of H_2/L_2 (in this situation, basically obtained by $(H_2/L_2)_{F,1o} = 0.2$). In addition, it is observed that the performance indicator $(\mathit{\Delta P}_{min,1o})$ has its performance decreased exponentially as the ratio H_1/L_1 increases, corroborating what was previously discussed and showing that lower values of H_1/L_1 bring the best performance benefits fluid dynamics of the problem. For the cases with $Re_H = 50$ and $Re_H = 100$ (Figs. 17b and 17c), it is observed that, from $H_1/L_1 \geq 1.0$, the optimal results for H_2/L_2 are obtained for ratios H_2/L_2 of greater magnitudes in relation to cases of $H_1/L_1 < 1.0$, since, in these situations, the increase in H_2/L_2 combined with the flow conditions minimizes the fluid dynamic resistance inside the system, producing slightly positive results. It is also noteworthy that, for all conditions evaluated (Re_H and H_1/L_1), the worst results were obtained for $(H_2/L_2)_{F,ws} = 6.0$, where the flow restriction caused by block 2 was maximum.

Figure 17 shows the percentage difference in the fluid dynamic performance with reference to the once optimized cases $((H_2/L_2)_{F,1o})$ in relation to the geometries that showed the lowest performance $((H_2/L_2)_{F,ws})$ in the system, as a function of H_1/L_1 for: (a) $Re_H = 10$; (b) $Re_H = 50$; and (c) $Re_H = 100$. As already observed in the thermal analyses of the problem, the importance of the geometric evaluation of the set of blocks through the Constructal Design method is also highlighted for the fluid dynamic assessment due to the great difference in performance between the optimal geometries and the cases of lower performance. In general terms, it is possible to observe that, for $0.1 \leq H_1/L_1 \leq 1.0$, the performance difference between the optimum cases and the lesser ones remains practically constant. In contrast, for $H_1/L_1 > 1$, this difference tends to decrease exponentially, since the obstruction given by block 1 becomes increasingly dominant in the system, causing the geometry of block 2 to lose relevance to the performance indicator $\mathit{\Delta P}$, leading to the optimal scenarios $((H_2/L_2)_{F,1o})$ to have their performances closer to the lower performance cases $((H_2/L_2)_{F,ws})$. Thus, for the cases evaluated by the flow given by $Re_H = 10$, where the performance differences between the geometries were smaller in relation to the other flow conditions studied, it is already possible to perceive a great increase in the performance of the optimized cases, obtaining improvements in the range of 72% to 240% in relation to the pressure variation inside the system.

For the cases under the conditions of $Re_H = 50$ and $Re_H = 100$, the performance of the optimum geometries $((H_2/L_2)_{F,1o})$ were even higher in relation to the geometries of lower performance $((H_2/L_2)_{F,ws})$, presenting gains in the thermal performance of the system in the range of 84% to 708% for $Re_H = 50$, and from 76% to 1275% for $Re_H = 100$.

In the second level of fluid dynamics optimization, the once optimized aspect ratio $(H_1/L_1)_{F,1o}$ and the twice optimized degree of freedom $((H_2/L_2)_{F,2o})$ (geometries that are indicated in Fig. 16) caused a significant increase in fluid dynamic performance, since the geometric configuration of the twice-optimized system presented results much superior when compared to the optimum geometries in the first optimization level, showing a great geometric influence of the blocks on the fluid dynamic performance indicator. Thus, for $Re_H = 10$, the twice optimized geometry $((H_1/L_1)_{F,1o} = 0.2$ and $(H_2/L_2)_{F,2o} = 0.2)$ presented superior results on the pressure drop inside the channel, obtaining an increase in system performance of up to 248% in relation to the lowest optimum performance of the system obtained in the first level of optimization $(H_1/L_1 = 6.0$ and $(H_2/L_2)_{F,1o} = 6.0)$. For $Re_H = 50$, the thermal gain of the twice optimized geometry $((H_1/L_1)_{F,1o} = 0.2$ and $(H_2/L_2)_{F,2o} = 0.2)$ was up to 635% in relation to $H_1/L_1 = 6.0$ and $(H_2/L_2)_{F,1o} = 6.0)$. Finally, for $Re_H = 100$, the performance increase was even greater, reaching a maximum of 1042% of the optimal geometry $((H_1/L_1)_{F,1o} = 0.2$ and $(H_2/L_2)_{F,2o} = 0.1)$ when compared to the optimum geometry of lower performance in a first optimization level $(H_1/L_1 = 6.0$ and $(H_2/L_2)_{F,1o} = 6.0)$.

Therefore, the multi-objective analysis of the problem was performed using the TOPSIS method. This methodology is used in systems with multiple performance objectives, as is the case of the present work, in which the objectives are (i) to maximize the heat transfer between the blocks and the fluid and (ii) minimize the pressure drop inside the channel. Fig. 18 shows the response surface for the multi-objective performance indicator (C_i) as a function of H_1/L_1 and H_2/L_2, for: (a) $Re_H = 10$; (b) $Re_H = 50$; and (c) $Re_H = 100$, calculated using the TOPSIS method. The geometries with the highest C_i values are closer to the ideal multi-objective solution. The weight of importance for the two objective functions of the problem was considered equal, where the variables w_1 and w_2 (Eq. 19) have their value defined as equal to 0.5 ($w_1 = w_2 = 0.5$). In this scenario, the results obtained by varying the two degrees of freedom (H_1/L_1 and H_2/L_2) were contemplated, and accordingly, the analysis of the multi-objective problem was developed at the second level of optimization.

For an adequate understanding of the surfaces presented in Fig. 18 and the factors that influence the multi-objective performance of the system, it is essential to evaluate the sensitivity of the performance indicators of the problem (maximization of $\tilde{q}$ and minimization of ΔP) concerning the geometric variation of the blocks. In the individual analysis of the thermal and fluid dynamics

25

problem, it was observed that the geometric variations across the degrees of freedom H_1/L_1 and H_2/L_2 within the studied range had a more substantial effect on the fluid dynamic performance of the system. This is verified since, for the fluid dynamic performance indicator ΔP, the difference in the geometry performance twice optimized in relation to the geometry with the lowest global performance of the system was approximately 498% for $Re_H = 10$, 1257% for $Re_H = 50$, and 1919% for $Re_H = 100$. These performance differences related to the thermal problem were noticeably smaller, approximately 49% for $Re_H = 10$, 106% for $Re_H = 50$, and 134% for $Re_H = 100$, showing a greater sensitivity fluid dynamics of the system with the geometric variation of the blocks. Therefore, in the surfaces of Fig. 18, it is observed that the worst multi-objective geometries, i.e., the ones that conduct to the lowest values of C_i, were found for the scenarios that presented the worst behavior of the solution regarding the fluid dynamic objective. These are given by the geometries that have the configurations of H_1/L_1 or H_2/L_2 with values greater than or equal to 5.0 (H_1/L_1; $H_2/L_2 \leq 5.0$).

In summary, these configurations are not feasible for the system in multi-objective criteria for the present studied conditions. From the moment when H_1/L_1 and H_2/L_2 have their values not exceeding 4.0 (H_1/L_1; $H_2/L_2 \leq 4.0$), the geometric freedom of the blocks starts to affect the performance less significantly from the fluid dynamic viewpoint, given that the difference between the best and the worst results related to ΔP was 85% for $Re_H = 10$, 164%, for $Re_H = 50$ and 230% for $Re_H = 100$. In this geometric region, the functions of $\tilde{q}$ and ΔP have a more balanced sensitivity to the variation of the degrees of freedom of the blocks, highlighting a more convenient region for multi-objective interest and presenting a plateau on the surfaces C_i shown in Fig. 18. This geometric region of interest is also represented through a two-dimensional geometric map colored about the performance C_i (see Fig. 18), which has adapted its color scale to better visualize the system's behavior for the multi-objective problem.

Because of this, for $Re_H = 10$ (Fig. 18a), the two-dimensional geometric map shows that the best multi-objective geometries are given for the system scenario where at least one of the blocks has its geometry (H_1/L_1 or H_2/L_2) defined by the aspect ratio of 2.0 or 3.0. These geometries have the highest values of C_i – represented by the red zone in the two-dimensional graph (being the combination with H_1/L_1 or H_2/L_2 equal to 5.0 and 6.0 an exception to this behavior). In addition, when drawing a line between the evaluated geometric extremes, symmetrical aspect to the multi-objective problem concerning the geometric variation of the blocks is perceived, where the regions of the graph marked by the letter 'F' represent the most beneficial multi-objective geometric zone for the fluid-dynamic criterion and the zone marked by 'T' represents a multi-objective geometric range more favorable for the thermal condition. For $Re_H = 50$ and $Re_H = 100$ (Figs. 18b and 18c), a

26

region of optimum multi-objective is observed, displaced where the blocks present their combined ratios in the range $2.0 \leq H_1/L_1$; $H_2/L_2 \leq 4.0$, since it was in this geometric region where an increase in thermal performance was identified, accompanied by an episodic reduction in pressure drop inside the channel (the situation that was previously discussed through Fig. 11), reaching the highest values of C_i. Furthermore, a multi-objective zone more focused on the thermal condition ('T') stands out in this region. In addition, it is possible to highlight the results obtained by the geometries given by $H_2/L_2 = 3.0$ and $H_2/L_2 = 4.0$, combined with $H_1/L_1 \leq 2.0$, which also presented high values of C_i when compared with the other studied geometric configurations, representing a good compromise condition on the multi-objective geometric shape of the system, more focused on the fluid dynamic criterion ('F').

To evaluate the performance of the optimal multi-objective geometric configuration in relation to the geometries twice optimized for a single criterion, thermal or fluid dynamic, Fig. 19 shows a comparison between the performances of the geometric sets optimized for the thermal $((H_1/L_1)_{T,1o}$; $(H_2/L_2)_{T,2o})$, fluid dynamic $((H_1/L_1)_{T,1o}$; $(H_2/L_2)_{F,2o})$ and multi-objective $((H_1/L_1)_{TMO,1o}$; $(H_2/L_2)_{TMO,2o})$ purposes, for: (a) $Re_H = 10$; (b) $Re_H = 50$; and (c) $Re_H = 100$, as a function of $\tilde{q}$ and ΔP. As previously analyzed, it is possible to observe which optimal multi-objective geometric set found through the TOPSIS method, for the different Reynolds numbers evaluated, had an intermediate performance compared to the geometric sets twice optimized for the thermal or fluid dynamic purpose only. Thus, in the condition of $Re_H = 10$ (Fig. 19a), the geometry considered to be optimal for the multi-objective problem $((H_1/L_1)_{TMO,1o} = 3.0$ and $(H_2/L_2)_{TMO,2o} = 1.0)$ showed a decrease in performance to the ideal thermal and fluid dynamic sets, losing a heat transfer capacity of approximately 29% in relation to the twice thermally optimized geometric set $((H_1/L_1)_{T,1o} = 6.0$ and $(H_2/L_2)_{T,2o} = 6.0)$, and 20% drop in performance in relation to the geometric set twice optimized for the fluid dynamic criterion $((H_1/L_1)_{F,1o} = 0.2$ and $(H_2/L_2)_{F,2o} = 0.2)$, in order to meet to a system that presented balanced performances in concerning the two criteria. As the Reynolds number increased (Figs. 19b and 19c), an even greater difference related to the comparative performance between the optimal multi-objective configurations with the ideal sets for thermal and fluid dynamics purposes was obtained, with magnitudes of approximately 47% and 65% to the optimum thermal, and approximately 110% and 152% to the optimum fluid-dynamics, for $Re_H = 50$ and $Re_H = 100$, respectively. Thus, for the studied flow conditions, it is observed that the increase in the Reynolds number caused a greater decrease in performance among the optimal multi-objective configurations concerning the geometric sets optimized specifically for the thermal or fluid-dynamic criteria. This result justifies the lower numbers of C_i obtained in Fig. 18 found for the

highest values of Re_H since the optimal multi-objective solution is farther from the ideal solutions (higher $\tilde{q}$ and lower ΔP) within the evaluated geometric set.

Additionally to the previous discussion, Fig. 20 presents the surfaces of multi-objective response (C_i) for different relevance of the system's thermal and fluid dynamic purposes (w_1 and w_2). This figure shows that, with the new weighting of the magnitude of the performance indicators, new geometric regions of great performance are defined for the multi-objective problem. Thus, new optimized configurations of H_1/L_1 and H_2/L_2 are established, adapting the block geometry to the new needs of the system. For situations in which greater thermal imposition is needed, the optimal multi-objective region shifts to the highest H_1/L_1 and H_2/L_2 values. As a counterpoint, when the need is for a system with greater fluid dynamics, the optimal geometric region is defined by the geometries with at least one degree of freedom, H_1/L_1 or H_2/L_2, close to its minimum value. Tables 5.1, 5.2, and 5.3 show the optimized geometries for the multi-objective problem, in which different weight values for w_1 and w_2 are considered.

Table 5 – Optimized geometries for the multi-objective problem obtained through the TOPSIS method for $Re_H = 10$ and different w_1 and w_2.

	$w_1(\%)$	$w_2(\%)$	$(H_1/L_1)_{Tmo,1o}$	$(H_2/L_2)_{Tmo,2o}$	$\tilde{q}$	ΔP
			$Re_H = 10$ and $Pr = 0.72$			
	95	5	5.0	6.0	6.0741	2.0567
	90	10	5.0	5.0	5.8375	1.3291
	85	15	5.0	4.0	5.6531	1.0922
Thermal relevance	80	20	4.0	4.0	5.4351	0.8570
	75	25	4.0	3.0	5.2592	0.7524
	70	30	4.0	3.0	5.2592	0.7524
	60	40	3.0	3.0	5.0504	0.6502
Balance	**50**	**50**	**3.0**	**0.1**	**4.8297**	**0.5579**
	40	60	2.0	0.1	4.6194	0.5055
	30	70	2.0	0.1	4.6194	0.5055
	25	75	2.0	0.1	4.6194	0.5055
Fluid dynamic relevance	20	80	0.1	0.2	4.4202	0.4636
	15	85	0.1	0.2	4.4202	0.4636
	10	90	0.1	0.2	4.4202	0.4636
	5	95	0.1	0.2	4.4202	0.4636

Table 6 – Optimized geometries for the multi-objective problem obtained through the TOPSIS method for $Re_H = 50$ and different w_1 and w_2.

$Re_H = 50$ and $Pr = 0.72$

	$w_1(\%)$	$w_2(\%)$	$(H_1/L_1)_{Tmo,1o}$	$(H_2/L_2)_{Tmo,2o}$	$\tilde{q}$	ΔP
	95	5	6.0	5.0	14.5582	21.0417
	90	10	6.0	5.0	14.5582	21.0417
	85	15	5.0	5.0	13.0362	12.1804
Thermal relevance	80	20	5.0	4.0	12.2464	8.7788
	75	25	5.0	4.0	12.2464	8.7788
	70	30	4.0	4.0	11.1823	6.2542
	60	40	4.0	3.0	10.4814	4.9801
Balance	**50**	**50**	**4.0**	**3.0**	**10.4814**	**4.9801**
	40	60	3.0	3.0	9.6861	3.9996
	30	70	0.1	2.0	8.5926	2.8101
	25	75	0.1	2.0	8.5926	2.8101
Fluid dynamic relevance	20	80	0.1	0.2	8.2658	2.3692
	15	85	0.1	0.2	8.2658	2.3692
	10	90	0.1	0.2	8.2658	2.3692
	5	95	0.1	0.2	8.2658	2.3692

Table 7 – Optimized geometries for the multi-objective problem obtained through the TOPSIS method for $Re_H = 100$ and different w_1 and w_2.

$Re_H = 100$ and $Pr = 0.72$						
	$w_1(\%)$	$w_2(\%)$	$(H_1/L_1)_{Tmo,1o}$	$(H_2/L_2)_{Tmo,2o}$	$\tilde{q}$	ΔP
	95	5	6.0	3.0	20.0902	57.8341
	90	10	6.0	3.0	20.0902	57.8341
	85	15	6.0	2.0	20.0437	57.4721
Thermal relevance	80	20	5.0	5.0	17.3487	34.2732
	75	25	5.0	3.0	16.2053	22.7488
	70	30	5.0	3.0	16.2053	22.7488
	60	40	4.0	4.0	14.7356	16.0841
Balance	**50**	**50**	**4.0**	**3.0**	**13.7225**	**12.2983**
	40	60	3.0	3.0	12.6751	9.3971
	30	70	3.0	3.0	12.6751	9.3971
	25	75	0.1	2.0	11.1656	6.3095
Fluid dynamic relevance	20	80	0.1	2.0	11.1656	6.3095
	15	85	0.1	0.2	10.5955	4.8721
	10	90	0.1	0.2	10.5955	4.8721
	5	95	0.1	0.2	10.5955	4.8721

4. CONCLUSIONS

This paper focuses on studying thermal and fluid dynamics effects in a system composed of a rectangular channel with heated semi-elliptical blocks inside. The evaluation was carried out using the Constructal Design associated with the Exhaustive Search and the TOPSIS method. The results were numerically simulated to determine the values of the aspect ratios H_1/L_1 and H_2/L_2 that maximize heat transfer between blocks inserted inside the channel and the surrounding fluid and minimize the pressure drop inside the channel. Allied to this, different flow conditions were studied, defined by $Re_H = 10$, $Re_H = 50$, $Re_H = 100$ and $Pr = 0.72$.

Many findings emerged from this work. As expected, the results regarding the thermal analysis of the system showed that the blocks with the best performance had the highest values of H_1/L_1 and H_2/L_2, i.e., greater height and obstruction of the channel. Also, the augmentation in the Reynolds number caused the thermal performance indicator to increase its sensitivity to the geometric variation of the blocks. It is also noteworthy that, for $Re_H = 50$ and $Re_H = 100$, the global thermal performance of the system fundamentally depends on the two blocks configuration, since the geometric set that presented the performance twice maximized thermally showed an almost equal heat dissipation between the heated blocks. On the other hand, for the flow defined by $Re_H = 10$, the maximum global performance was essentially influenced by the upstream block in the system (block 1), since the low magnitude of the flow, given the high channel obstruction caused by block 1, resulted in a predominance of the heat diffusion effects in the system, impairing the participation in the heat transfer of the block positioned downstream of the flow (block 2).

Regarding the fluid dynamics analysis of the system, the best global results were obtained for the geometries that presented a lower obstruction of the flow inside the channel, i.e., the lower values of H_1/L_1 and H_2/L_2. In addition, the increase in the Reynolds number led the system to a more significant difference in performance between the twice optimized geometries and the poorer performance geometries obtained, significantly increasing the geometric sensitivity of the system concerning the fluid dynamic indicator.

For the multi-objective assessment of the problem, the TOPSIS method was applied to define the optimal geometric configurations that could contemplate both the instances, i.e., the thermal and fluid dynamics objectives. As expected, the best results for the multi-objective problem were obtained for intermediate geometric sets, and it was possible to formulate a recommendation of optimal multi-objective geometry for the system through Constructal Design associated with the TOPSIS method. Besides, the regions of excellent multi-objective scenarios have been proposed within the geometrical spectrum studied, highlighting geometries with a good multi-objective level and slight thermal or fluid dynamics preference. These results show that systems with more than one component must be evaluated together to obtain adequate performance maximization.

Finally, the present study showed the importance of Constructal Design for the evaluation of the proposed thermal and fluid dynamics problem, so that the system design presented optimal and morphing geometric configurations, which were being modified as the performance indicator was changed, resembling the form of generating design in systems found in nature.

Acknowledgements

REFERENCES

[1] Young, T. J., & Vafai, K. (1998). Convective cooling of a heated obstacle in a channel. *International Journal of Heat and Mass Transfer*, 4*1*(20), 3131-3148.

[2] Bar-Cohen, A., and Rohsenow, W. M. (February 1, 1984). "Thermally Optimum Spacing of Vertical, Natural Convection Cooled, Parallel Plates." ASME. *J. Heat Transfer*. February 1984; 106(1): 116–123.

[3] Dogan, A., Sivrioglu, M., & Baskaya, S. (2006). Investigation of mixed convection heat transfer in a horizontal channel with discrete heat sources at the top and at the bottom. *International Journal of Heat and Mass Transfer*, *49*(15-16), 2652-2662.

[4] Korichi, A., & Oufer, L. (2005). Numerical heat transfer in a rectangular channel with mounted obstacles on upper and lower walls. *International Journal of Thermal Sciences*, *44*(7), 644-655.

[5] Pishkar, I., & Ghasemi, B. (2012). Cooling enhancement of two fins in a horizontal channel by nanofluid mixed convection. *International Journal of Thermal Sciences*, *59*, 141-151.

[6] Handoyo, E. A., & Ichsani, D. (2016). Numerical studies on the effect of delta-shaped obstacles' spacing on the heat transfer and pressure drop in v-corrugated channel of solar air heater. *Solar Energy*, *131*, 47-60.

[7] Salcedo, E., Treviño, C., Palacios-Morales, C., Zenit, R., & Martínez-Suástegui, L. (2017). Experimental study on laminar flow over two confined isothermal cylinders in tandem during mixed convection. *International Journal of Thermal Sciences*, *115*, 176-196.

[8] Zheng, D., Wang, X., & Yuan, Q. (2019). The flow and heat transfer characteristics in a rectangular channel with convergent and divergent slit ribs. *International Journal of Heat and Mass Transfer*, *141*, 464-475.

[9] Liu, J., Hussain, S., Wang, W., Wang, L., Xie, G., & Sundén, B. (2019). Heat transfer enhancement and turbulent flow in a rectangular channel using perforated ribs with inclined holes. *Journal of Heat Transfer*, *141*(4).

[10] Li, X., Xie, G., Liu, J., & Sunden, B. (2020). Parametric study on flow characteristics and heat transfer in rectangular channels with strip slits in ribs on one wall. *International Journal of Heat and Mass Transfer*, *149*, 118396.

[11] Ghaneifar, M., Raisi, A., Ali, H. M., & Talebizadehsardari, P. (2021). Mixed convection heat transfer of AL 2 O 3 nanofluid in a horizontal channel subjected with two heat sources. *Journal of Thermal Analysis and Calorimetry*, *143*(3), 2761-2774.

[12] Davalath, J., and Bayazitoglu, Y. (May 1, 1987). "Forced Convection Cooling Across Rectangular Blocks." ASME. *J. Heat Transfer*. May 1987; 109(2): 321–328.

[13] Guimarães, P. M., & Menon, G. J. (2008). Combined free and forced convection in an inclined channel with discrete heat sources. *International Communications in Heat and Mass Transfer*, *35*(10), 1267-1274.

[14] Boutina, L., & Bessaïh, R. (2011). Numerical simulation of mixed convection air-cooling of electronic components mounted in an inclined channel. *Applied Thermal Engineering*, *31*(11-12), 2052-2062.

[15] Esfe, M. H., Arani, A. A. A., Niroumand, A. H., Yan, W. M., & Karimipour, A. (2015). Mixed convection heat transfer from surface-mounted block heat sources in a horizontal channel with nanofluids. *International Journal of Heat and Mass Transfer*, *89*, 783-791.

[16] Durgam, S., Venkateshan, S. P., & Sundararajan, T. (2017). Experimental and numerical investigations on optimal distribution of heat source array under natural and forced convection in a horizontal channel. *International Journal of Thermal Sciences*, *115*, 125-138.

[17] Wang, G., Chen, T., Tian, M., & Ding, G. (2020). Fluid and heat transfer characteristics of microchannel heat sink with truncated rib on sidewall. *International Journal of Heat and Mass Transfer*, *148*, 119142.

[18] Anirudh, K., & Dhinakaran, S. (2020). Performance improvement of a flat-plate solar collector by inserting intermittent porous blocks. *Renewable Energy*, *145*, 428-441.

[19] Hssain, M. A., Mir, R., & El Hammami, Y. (2020). Numerical Simulation of the cooling of heated electronic blocks in horizontal channel by mixed convection of nanofluids. *Journal of Nanomaterials*, *2020*.

[20] Bouabdallah, S., Ghernaout, B., Bellaouar, A., Bouras, A., & Ghazel, A. (2020). 3D Forced Convection in a Box Containing Two Cylindrical Heat Sources. *Advances in Modelling and Analysis B*, *63*(1-4), 20-25.

[21] Chati, D., Bouabdallah, S., Ghernaout, B., Tunçbilek, E., Arıcı, M., & Driss, Z. (2021). Turbulent mixed convective heat transfer in a ventilated enclosure with a cylindrical/cubical heat source: a 3D analysis. *Energy Sources, Part A: Recovery, Utilization, and Environmental Effects*, 1-18.

[22] Brauer, H. (1964) "Compact heat exchangers". *Chemical and Process Engineering*, 451-460.

[23] Rocha, L. A. O., Saboya, F. E. M., & Vargas, J. V. C. (1997). A comparative study of elliptical and circular sections in one-and two-row tubes and plate fin heat exchangers. *International Journal of Heat and Fluid Flow*, *18*(2), 247-252.

[24] Razera, A. L., da Fonseca, R. J. C., Isoldi, L. A., dos Santos, E. D., Rocha, L. A. O., & Biserni, C. (2018). Constructal design of a semi-elliptical fin inserted in a lid-driven square cavity with mixed convection. *International Journal of Heat and Mass Transfer*, *126*, 81-94.

[25] Chapman, C. L., Lee, S., & Schmidt, B. L. (1994, February). Thermal performance of an elliptical pin fin heat sink. In *Proceedings of 1994 IEEE/CHMT 10th Semiconductor Thermal Measurement and Management Symposium (SEMI-THERM)* (pp. 24-31). IEEE.

[26] Jang, J. Y., & Yang, J. Y. (1998). Experimental and 3-D numerical analysis of the thermal-hydraulic characteristics of elliptic finned-tube heat exchangers. *Heat Transfer Engineering*, *19*(4), 55-67.

[27] Faruquee, Z., Ting, D. S., Fartaj, A., Barron, R. M., & Carriveau, R. (2007). The effects of axis ratio on laminar fluid flow around an elliptical cylinder. *International Journal of Heat and Fluid Flow*, *28*(5), 1178-1189.

[28] Ibrahim, T. A., & Gomaa, A. (2009). Thermal performance criteria of elliptic tube bundle in crossflow. *International Journal of Thermal Sciences*, *48*(11), 2148-2158.

[29] Seyf, H. R., & Layeghi, M. (2010). Numerical analysis of convective heat transfer from an elliptic pin fin heat sink with and without metal foam insert. *Journal of Heat Transfer*, *132*(7).

[30] Liao, C. C., & Lin, C. A. (2012). Influences of a confined elliptic cylinder at different aspect ratios and inclinations on the laminar natural and mixed convection flows. *International journal of heat and mass transfer*, *55*(23-24), 6638-6650.

[31] Hermany, L., Lorenzini, G., Klein, R. J., Zinani, F. F., Dos Santos, E. D., Isoldi, L. A., & Rocha, L. A. O. (2018). Constructal design applied to elliptic tubes in convective heat transfer cross-flow of viscoplastic fluids. *International Journal of Heat and Mass Transfer*, *116*, 1054-1063.

[32] Gangawane, K. M., & Gupta, S. (2018). Mixed convection characteristics in rectangular enclosure containing heated elliptical block: Effect of direction of moving wall. *International Journal of Thermal Sciences*, *130*, 100-115.

[33] Nemati, H., Moradaghay, M., Moghimi, M. A., & Meyer, J. P. (2020). Natural convection heat transfer over horizontal annular elliptical finned tubes. *International Communications in Heat and Mass Transfer*, *118*, 104823.

[34] Wang, Y., Zhao, W., Wang, P., Jiang, J., & Luo, X. (2021). Thermal Performance of Elliptical Fin-and-Tube Heat Exchangers with Vortex Generator under Various Inclination Angles. *Journal of Thermal Science*, *30*(1), 257-270.

[35] Matos, R. S., Vargas, J. V. C., Rossetim, M. A., Pereira, M. V. A., Pitz, D. B., & Ordonez, J. C. (2021). Performance comparison of tube and plate-fin circular and elliptic heat exchangers for HVAC-R systems. *Applied Thermal Engineering*, *184*, 116288.

[36] Selimefendigil, F. (2019). Mixed convection in a lid-driven cavity filled with single and multiple-walled carbon nanotubes nanofluid having an inner elliptic obstacle. *Propulsion and Power Research*, *8*(2), 128-137.

[37] Javadzadegan, A., Joshaghani, M., Moshfegh, A., Akbari, O. A., Afrouzi, H. H., & Toghraie, D. (2020). Accurate meso-scale simulation of mixed convective heat transfer in a porous media for a vented square with hot elliptic obstacle: an LBM approach. *Physica A: Statistical Mechanics and its Applications*, *537*, 122439.

[38] Bejan, A., & Lorente, S. (2008). Design with Constructal Theory. *In: Shape and Thermodynamics, International Workshop Florence 2008*, 25-26 September 2008, Florence.

[39] Bejan, A. (2000). **Shape and structure, from engineering to nature.** Cambridge university press.

[40] Bejan, A., &; Lorente, S. (2006). Constructal theory of generation of configuration in nature and engineering. *Journal of applied physics*, 100(4), 5.

[41] Bejan, A., And Zane, J. P. (2012). **Design in Nature**, Doubleday, New York.

[42] Bejan, A., & Lorente, S. (2013). Constructal law of design and evolution: Physics, biology, technology, and society. *Journal of Applied Physics*, *113*(15), 6.

[43] Bejan, A. (2018). Thermodynamics today. *Energy*, *160*, 1208-1219.

[44] Bejan, A. (2020). **Freedom and evolution: hierarchy in nature, society, and science**. Springer Nature.

[45] Bello-Ochende, T., & Bejan, A. (2005). Constructal multi-scale cylinders in cross-flow. *International Journal of Heat and Mass Transfer*, *48*(7), 1373-1383.

[46] Bello-Ochende, T., Meyer, J. P., & Ogunronbi, O. I. (2011). Constructal multiscale cylinders rotating in cross-flow. *International Journal of Heat and Mass Transfer*, *54*(11-12), 2568-2577.

[47] Kim, Y., Lorente, S., & Bejan, A. (2010). Constructal multi-tube configuration for natural and forced convection in cross-flow. *International Journal of Heat and Mass Transfer*, *53*(23-24), 5121-5128.

[48] Teixeira, F. B., Lorenzini, G., Errera, M. R., Rocha, L. A. O., Isoldi, L. A., & Dos Santos, E. D. (2018). Constructal Design of triangular arrangements of square bluff bodies under forced convective turbulent flows. *International Journal of Heat and Mass Transfer*, *126*, 521-535.

[49] Razera, A. L., Quezada, L. A., Fagundes, T. M., Isoldi, L. A., dos Santos, E. D., Biserni, C., & Rocha, L. A. O. (2019). Fluid flow and heat transfer maximization of elliptic cross-section tubes exposed to forced convection: A numerical approach motivated by Bejan's theory. *International Communications in Heat and Mass Transfer*, *109*, 104366.

[50] Feijó, B. C., Lorenzini, G., Isoldi, L. A., Rocha, L. A. O., Goulart, J. N. V., & Dos Santos, E. D. (2018). Constructal design of forced convective flows in channels with two alternated rectangular heated bodies. *International Journal of Heat and Mass Transfer*, *125*, 710-721.

[51] Teixeira, F. B., Altnetter, M. V., Lorenzini, G., Rodriguez, B. D. A., Rocha, L. A. O., Isoldi, L. A., & Dos Santos, E. D. (2020). Geometrical evaluation of a channel with alternated mounted blocks under mixed convection laminar flows using Constructal Design. *Journal of Engineering Thermophysics*, *29*(1), 92-113.

[52] Rocha, L. A. O., Lorente, S., & Bejan, A. (2002). Constructal design for cooling a disc-shaped area by conduction. *International Journal of Heat and Mass Transfer*, *45*(8), 1643-1652.

[53] Rocha, L. A., Lorente, S., & Bejan, A. (2006). Conduction tree networks with loops for cooling a heat generating volume. *International journal of heat and mass transfer*, *49*(15-16), 2626-2635.

[54] Lorenzini, G., & Rocha, L. A. O. (2009). Geometric optimization of TY-shaped cavity according to constructal design. *International Journal of heat and mass transfer*, *52*(21-22), 4683-4688.

[55] Azarkish, H., Sarvari, S. M. H., & Behzadmehr, A. (2010). Optimum design of a longitudinal fin array with convection and radiation heat transfer using a genetic algorithm. *International Journal of Thermal Sciences*, *49*(11), 2222-2229.

[56] Hajmohammadi, M. R. (2017). Introducing a ψ-shaped cavity for cooling a heat generating medium, *International Journal of Thermal Sciences*. 121 204–212,

[57] Biserni, C., Dalpiaz, F. L., Fagundes, T. M., & Rocha, L. A. O. (2017). Constructal design of T-shaped morphing fins coupled with a trapezoidal basement: a numerical investigation by means of exhaustive search and genetic algorithm. *International Journal of Heat and Mass Transfer*, *109*, 73-81.

[58] Hajmohammadi, M. R. (2018). Optimal design of tree-shaped inverted fins. *International Journal of Heat and Mass Transfer*, *116*, 1352-1360.

[59] Fagundes, T. M., Lorenzini, G., da SD Estrada, E., Isoldi, L. A., Dos Santos, E. D., Rocha, L. A. O., & da Silva Neto, A. J. (2019). Constructal design of conductive asymmetric tri-forked pathways. *Journal of Engineering Thermophysics*, *28*(1), 26-42.

[60] Xie, G., Zhang, F., Sundén, B., & Zhang, W. (2014). Constructal design and thermal analysis of microchannel heat sinks with multistage bifurcations in single-phase liquid flow. *Applied thermal engineering*, *62*(2), 791-802.

[61] Mustafa, A. W. (2019). Constructal design of multi-scale diamond-shaped pin fins cooled by mixed convection. *International Journal of Thermal Sciences*, *145*, 106018.

[62] Rocha, L. A. O., Lorenzini, G., Biserni, C., & Cho, Y. (2010). Constructal design of a cavity cooled by convection. *International Journal of Design & Nature and Ecodynamics*, *5*(3), 212-220.

[63] Rodrigues, P. M., Biserni, C., De Escobar, C. C., Rocha, L. A. O., Isoldi, L. A., & Dos Santos, E. D. (2020). Geometric optimization of a lid-driven cavity with two rectangular intrusions under mixed convection heat transfer: A numerical investigation motivated by constructal design. *International Communications in Heat and Mass Transfer*, *117*, 104759.

[64] Razera, A. L., Fagundes, T. M., Seibt, F. M., da Fonseca, R. J., Varela, D. J., Ortiz, P. R., ... & Rocha, L. A. O. (2016). Constructal Design of a Triangular Fin Inserted in a Cavity with Mixed Convection Lid-Driven Flow. In *Defect and Diffusion Forum* (Vol. 372, pp. 188-201). Trans Tech Publications Ltd.

[65] Vieira, R. S., Petry, A. P., Rocha, L. A. O., Isoldi, L. A., & Dos Santos, E. D. (2017). Numerical evaluation of a solar chimney geometry for different ground temperatures by means of constructal design. *Renewable Energy*, *109*, 222-234.

[66] Martins, J. C., Goulart, M. M., Gomes, M. D. N., Souza, J. A., Rocha, L. A. O., Isoldi, L. A., & Dos Santos, E. D. (2018). Geometric evaluation of the main operational principle of an overtopping wave energy converter by means of Constructal Design. *Renewable Energy*, *118*, 727-741.

[67] Gomes, M. D. N., Lorenzini, G., Rocha, L. A. O., Dos Santos, E. D., & Isoldi, L. A. (2018). Constructal design applied to the geometric evaluation of an oscillating water column wave energy converter considering different real scale wave periods. *Journal of Engineering Thermophysics*, *27*(2), 173-190.

[68] Klein, R. J., Zinani, F. S. F., Rocha, L. A. O., & Biserni, C. (2018). Effect of Bejan and Prandtl numbers on the design of tube arrangements in forced convection of shear thinning fluids: a numerical approach motivated by constructal theory. *International Communications in Heat and Mass Transfer*, *93*, 74-82.

[69] Hwang, C. L., & Yoon, K. (1981). Methods for multiple attribute decision making. In *Multiple attribute decision making* (pp. 58-191). Springer, Berlin, Heidelberg.

[70] Trilok, G., & Gnanasekaran, N. (2021). Numerical study on maximizing heat transfer and minimizing flow resistance behavior of metal foams owing to their structural properties. *International Journal of Thermal Sciences*, *159*, 106617.

[71] Ge, Y., Liu, Z., & Liu, W. (2016). Multi-objective genetic optimization of the heat transfer for tube inserted with porous media. *International Journal of Heat and Mass Transfer*, *101*, 981-987.

[72] Mao, N., Song, M., & Deng, S. (2016). Application of TOPSIS method in evaluating the effects of supply vane angle of a task/ambient air conditioning system on energy utilization and thermal comfort. *Applied Energy*, *180*, 536-545.

[73] Versteeg, H. K., & Malalasekera, W. (2007). **An introduction to computational fluid dynamics: the finite volume method**. Pearson education.

[74] Patankar, S. (2018). **Numerical heat transfer and fluid flow**. Taylor & Francis.

[75] FLUENT (2011), version 14.0, User's guide, Ansys Inc.

[76] Bejan, A. (2013). **Convection heat transfer**. John Wiley & Sons.

[77] Schlichting, H.; Gersten, K. "**Boundary-Layer Theory**". Springer, 2016

[78] dos Santos, E. D., Isoldi, L. A., Gomes, M. D. N., & Rocha, L. A. (2017). The constructal design applied to renewable energy systems. *Sustainable Energy Technologies*, *1*(4), 63-87.

[79] Churchill, S. W., and Bernstein, M. (May 1, 1977). "A Correlating Equation for Forced Convection from Gases and Liquids to a Circular Cylinder in Crossflow." ASME. *J. Heat Transfer*. May 1977; 99(2): 300–306.

[80] Hilpert, R. (1933). Heat transfer from cylinders. *Forsch. Geb. Ingenieurwes*, *4*(5), 215.

[81] Khan, W. A., Culham, J. R., & Yovanovich, M. M. (2004). Fluid flow and heat transfer from a cylinder between parallel planes. *Journal of thermophysics and heat transfer*, *18*(3), 395-403.

[82] Incropera, F. P., Lavine, A. S., Bergman, T. L., & DeWitt, D. P. (2007). **Fundamentals of heat and mass transfer. Wiley.**
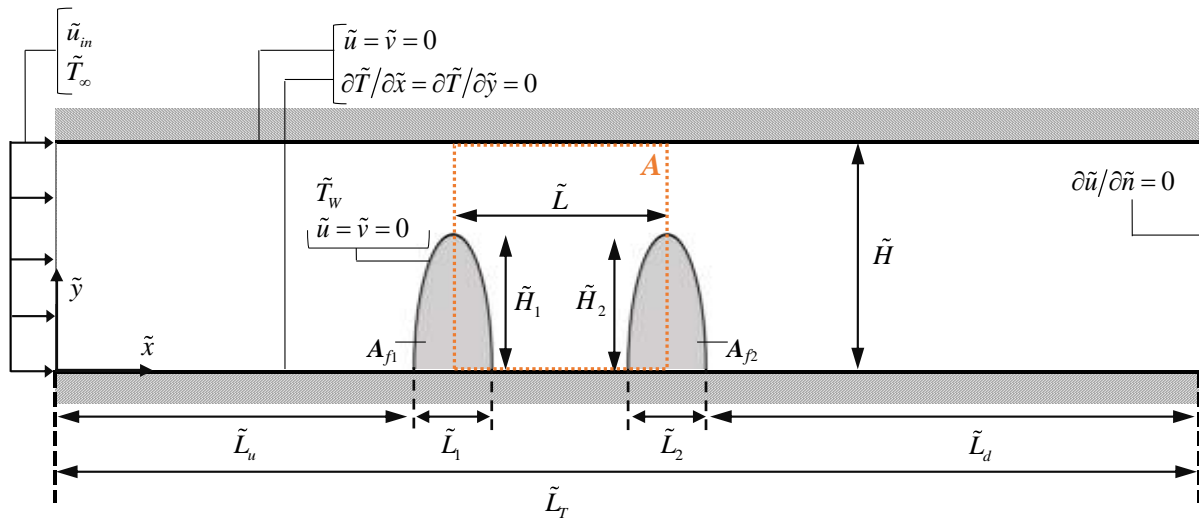
Figure 1 – Schematic representation of the domain with boundary conditions.
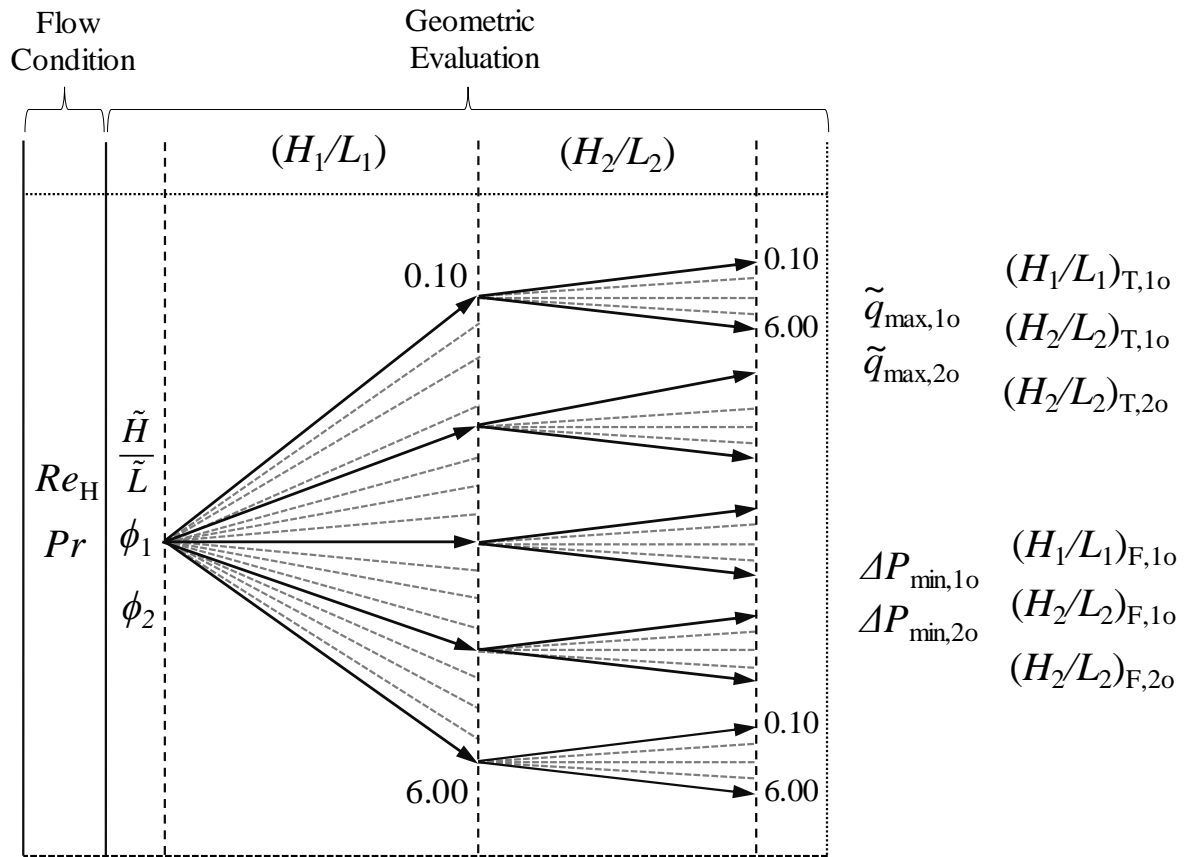
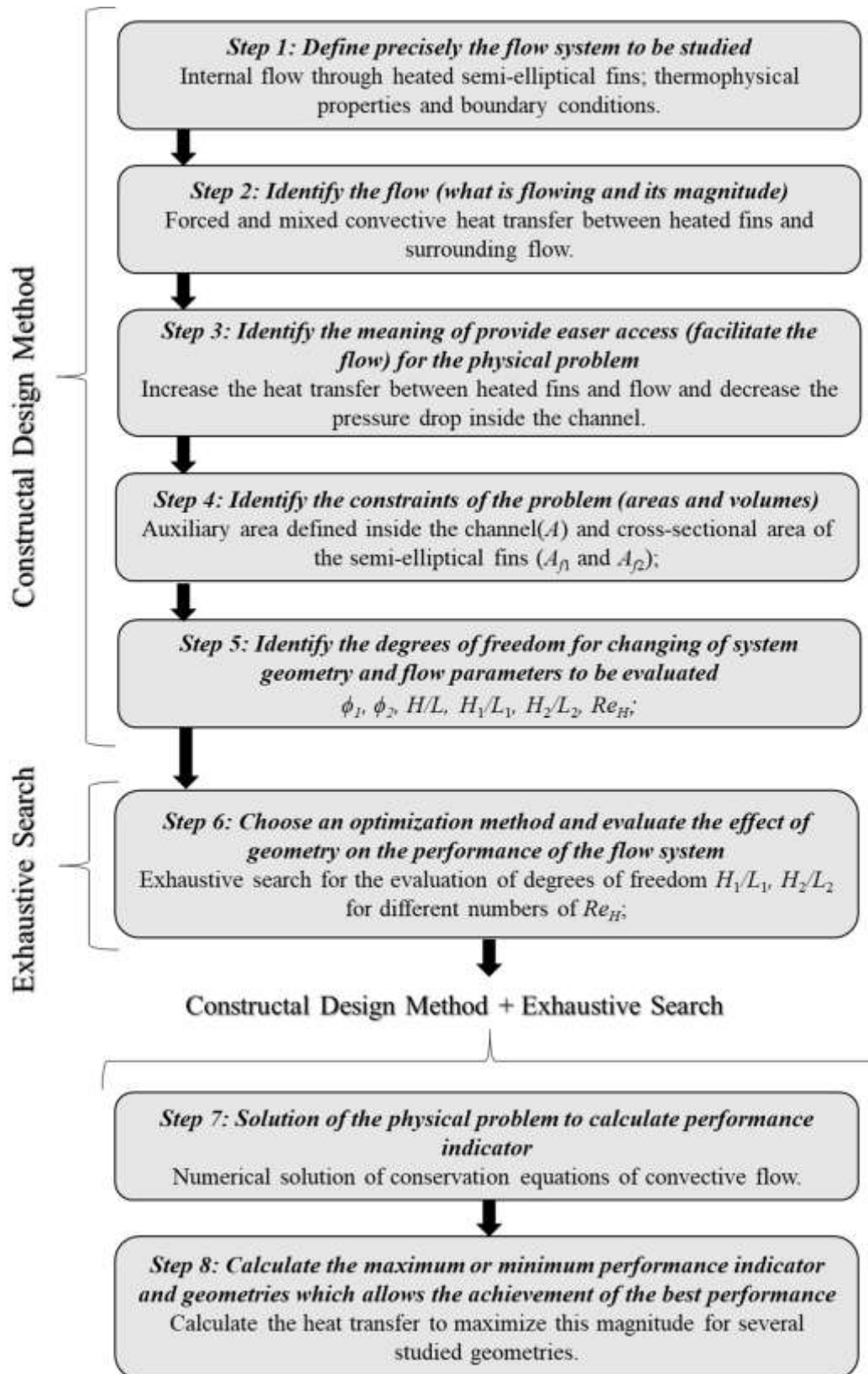Figure 2 – Representative scheme of the Constructal Design method associated with the Exhaustive Search mechanism.

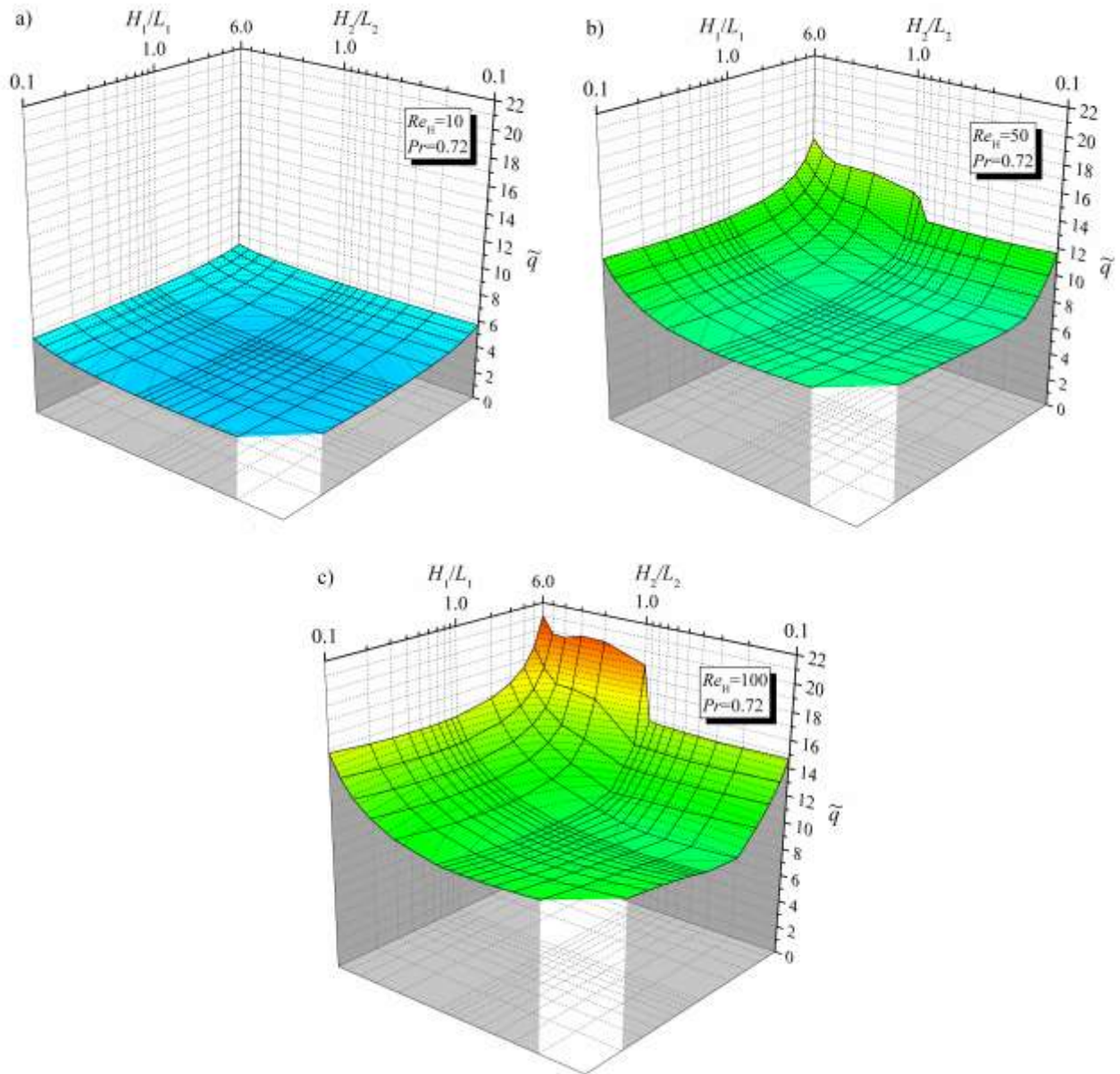Figure 3 – Flowchart with the application of Constructal Design method associated with Exhaustive Search [76].

Figure 4 – Study of total dimensionless heat transfer ($\tilde{q}$) as a function of the degrees of freedom H_1/L_1 and H_2/L_2 for different Reynolds numbers: (a) $Re_H = 10$; (b) $Re_H = 50$; (c) $Re_H = 100$.

41
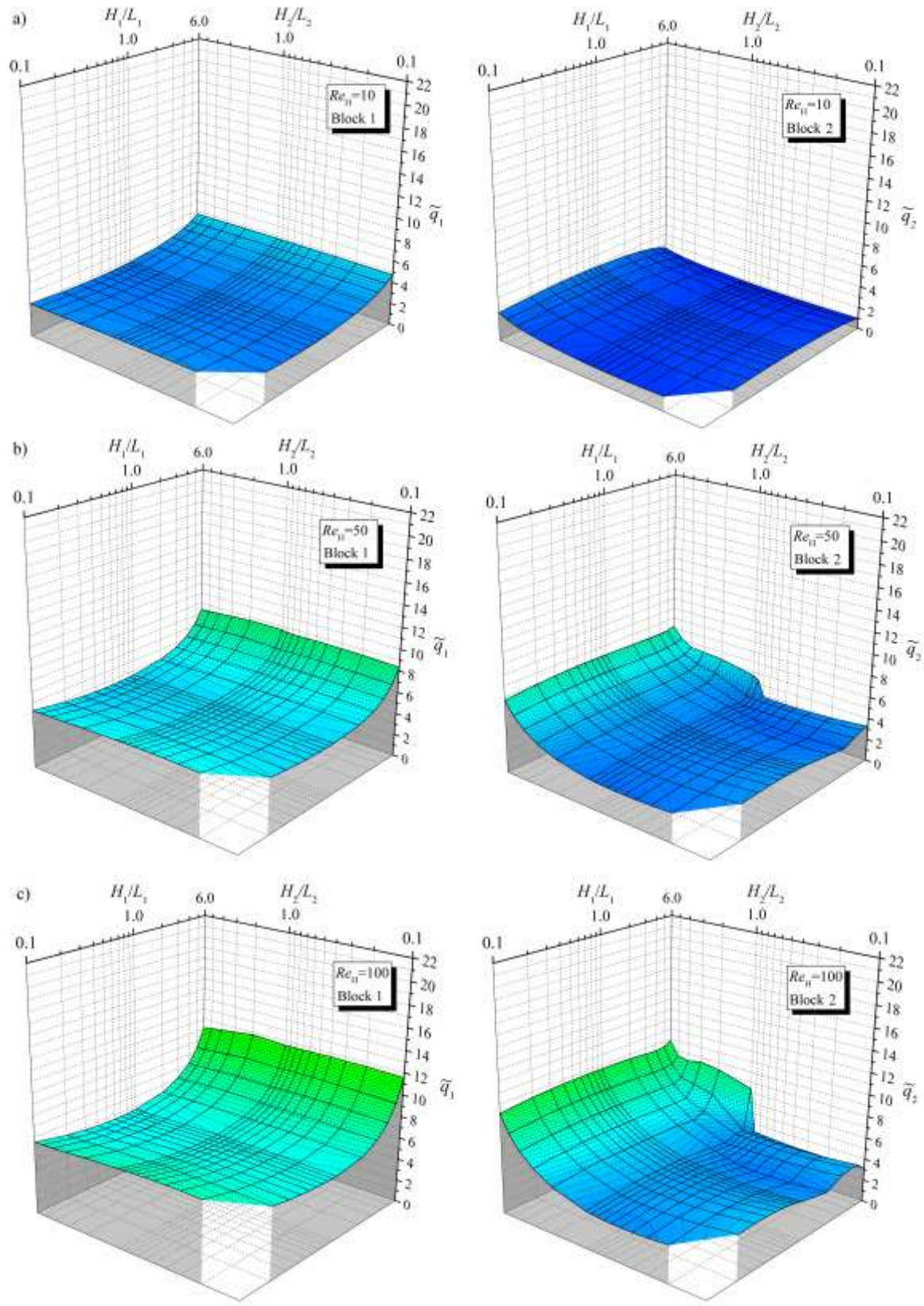
Figure 5 – Study of individual dimensionless heat transfer of the blocks ($\tilde{q}_1$ and $\tilde{q}_2$) as a function of the degrees of freedom H_1/L_1 and H_2/L_2 for different Reynolds numbers: (a) $Re_H = 10$; (b) $Re_H = 50$; (c) $Re_H = 100$.

42
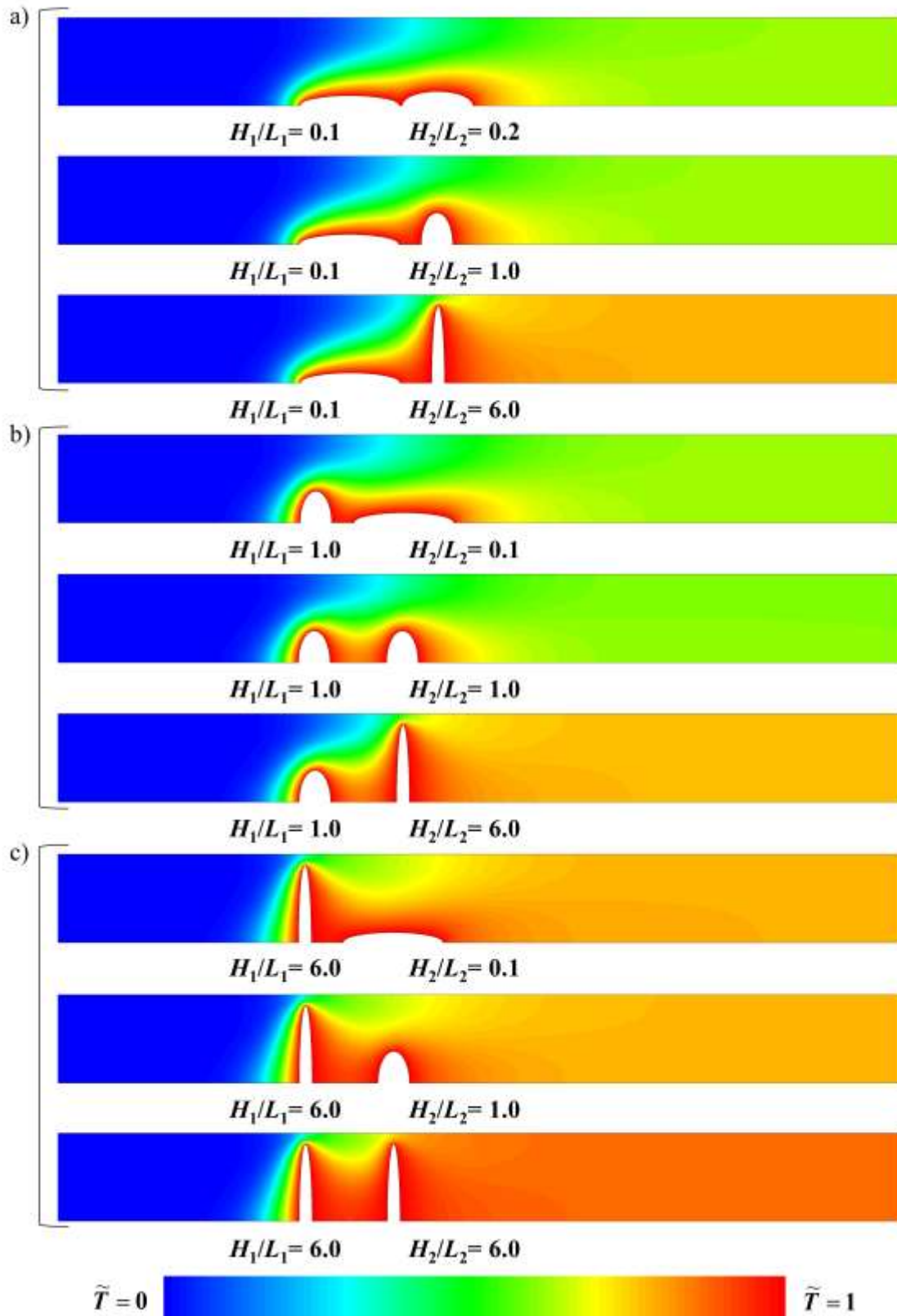
Figure 6 – Temperature fields for a set of blocks geometries within the channel considering $Re_H =10$ and $Pr = 0.72$ for: (a) $H_1/L_1= 0.1$; (b) $H_1/L_1 = 1.0$; (c) $H_1/L_1= 6.0$.
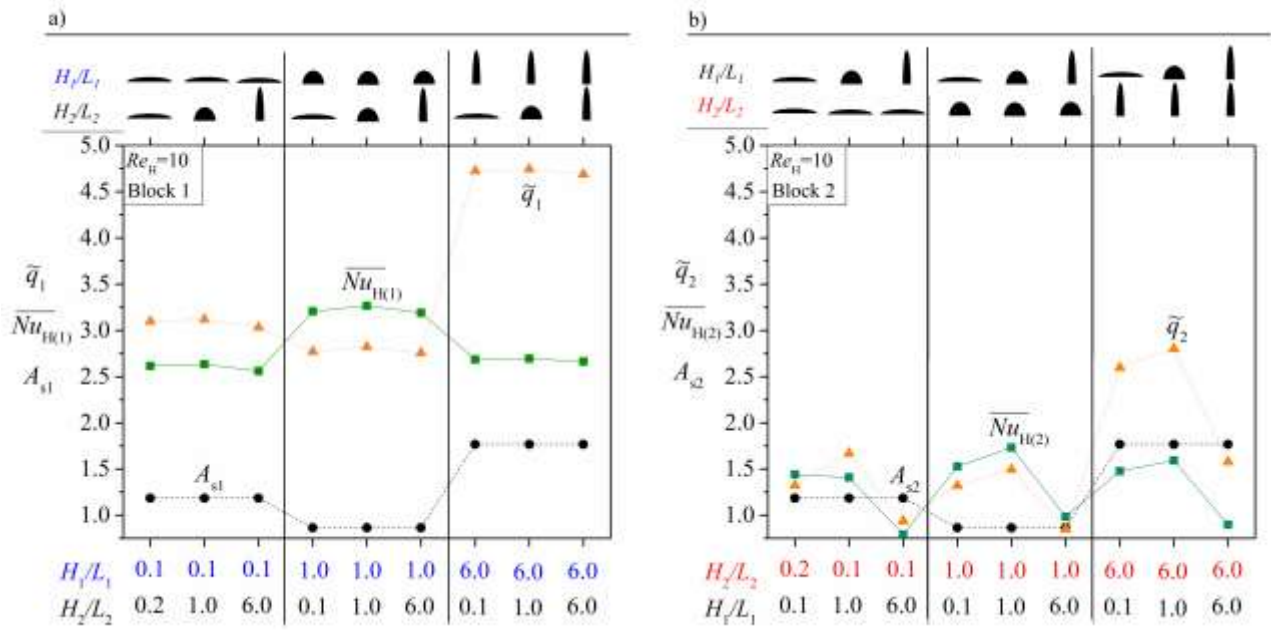
Figure 7 – Individual thermal performance of the blocks for a set of geometries evaluated in the flow with $Re_H = 10$ for (a) Block 1; (b) Block 2.
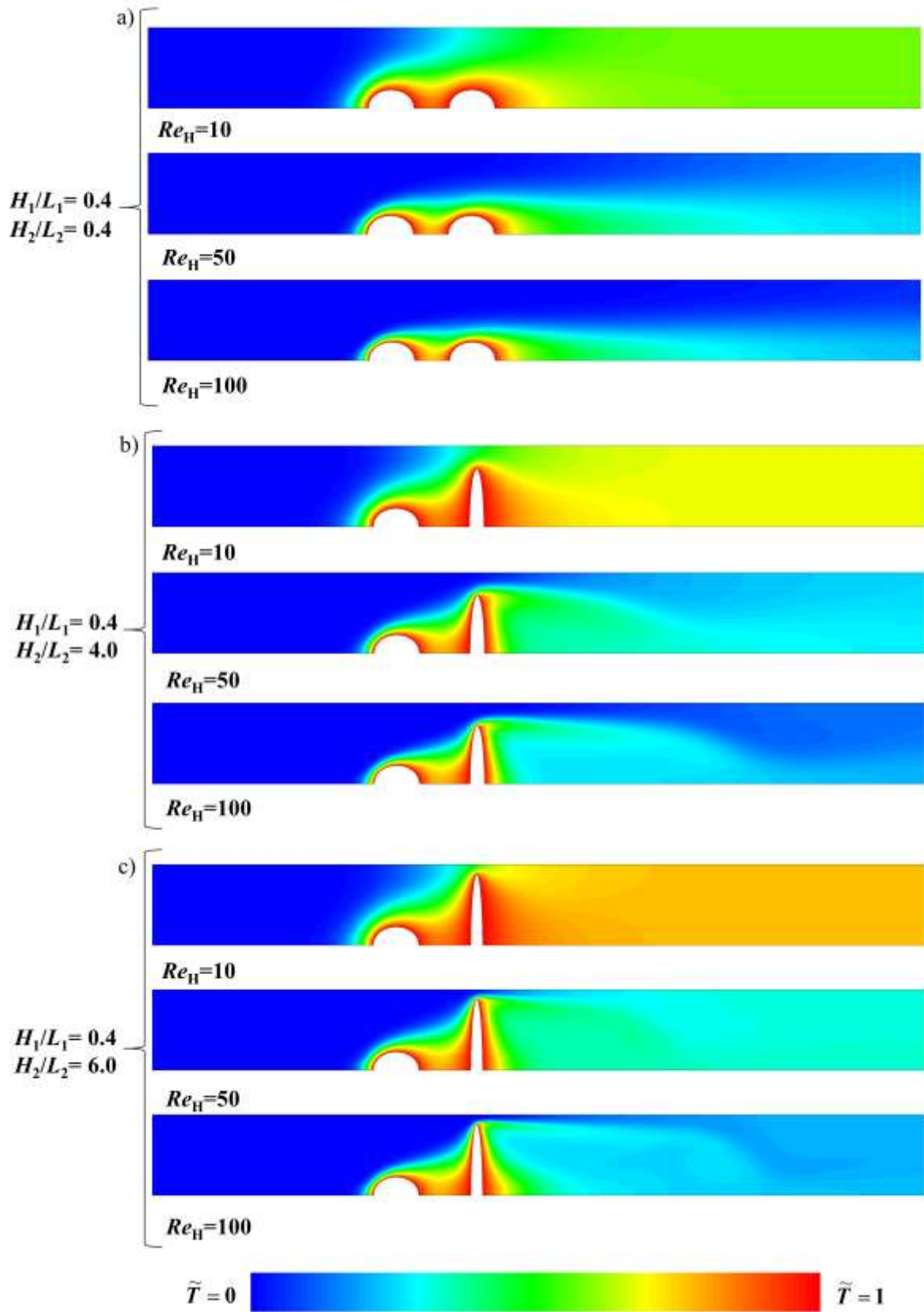
Figure 8 – Temperature fields considering the different Re_H evaluated for: (a) $H_1/L_1 = 0.4$ and H_2/L_2 = 0.4; (b) $H_1/L_1 = 0.4$ and $H_2/L_2 = 6.0$.
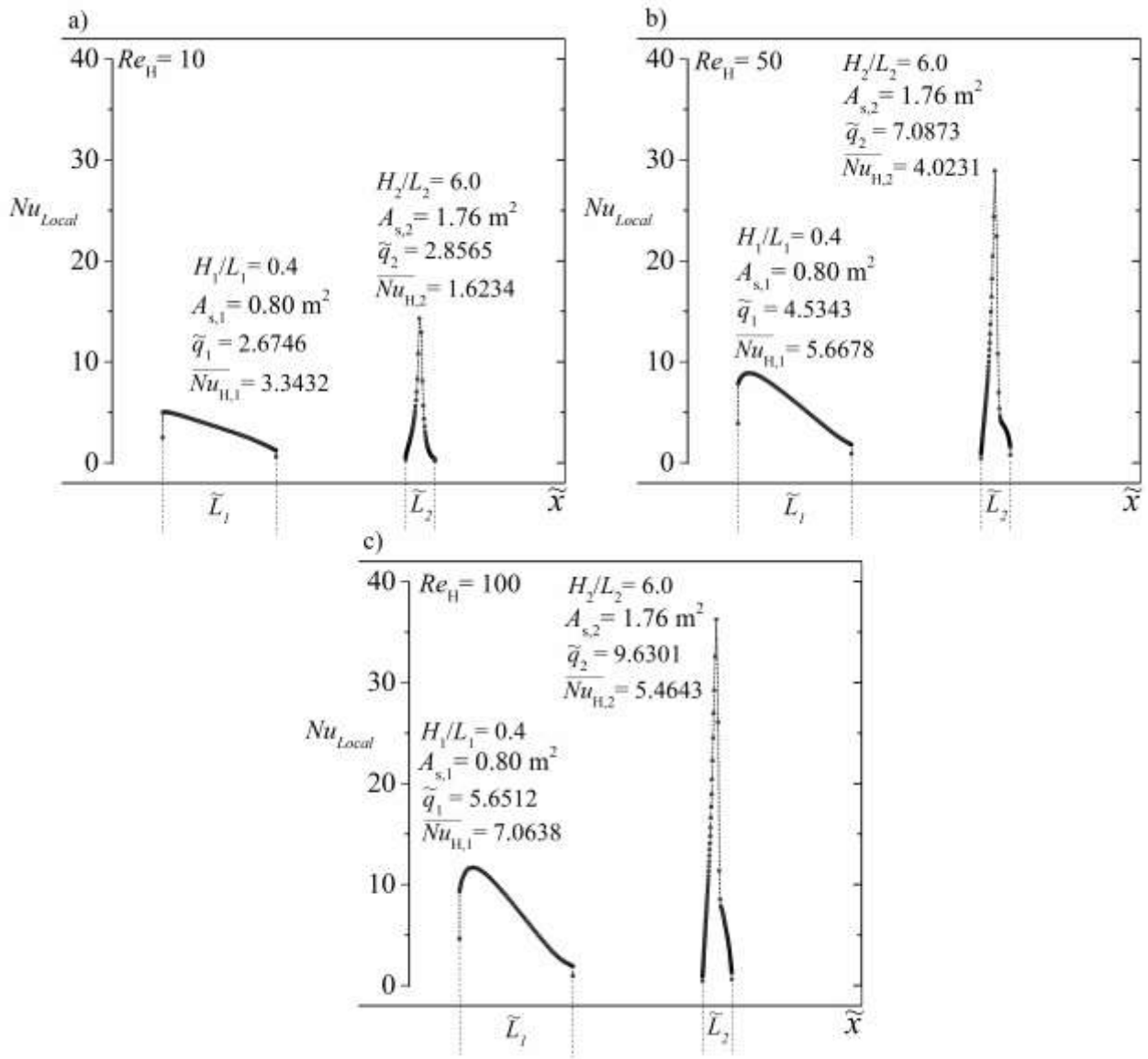
Figure 9 – Effects of the local heat transfer (Nu_{Local}) on the surfaces of blocks 1 and 2 for the geometric configurations given by $H_1/L_1 = 0.4$ and $H_2/L_2 = 6.0$, and (a) $Re_H = 10$; (b) $Re_H = 50$; (c) $Re_H = 100$.
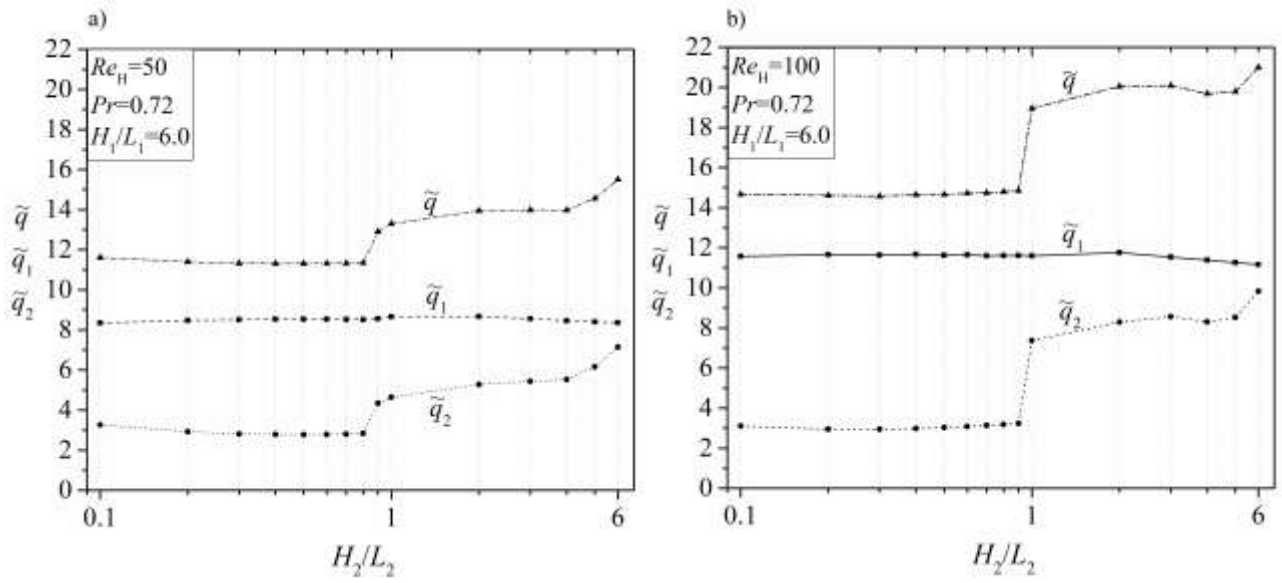
Figure 10 – Dimensionless heat transfer, $\tilde{q}$, $\tilde{q}_1$ and $\tilde{q}_2$, as a function of the degree of freedom H_2/L_2 considering $H_1/L_1 = 6.0$ fixed for: (a) $Re_H = 50$; (b) $Re_H = 100$.
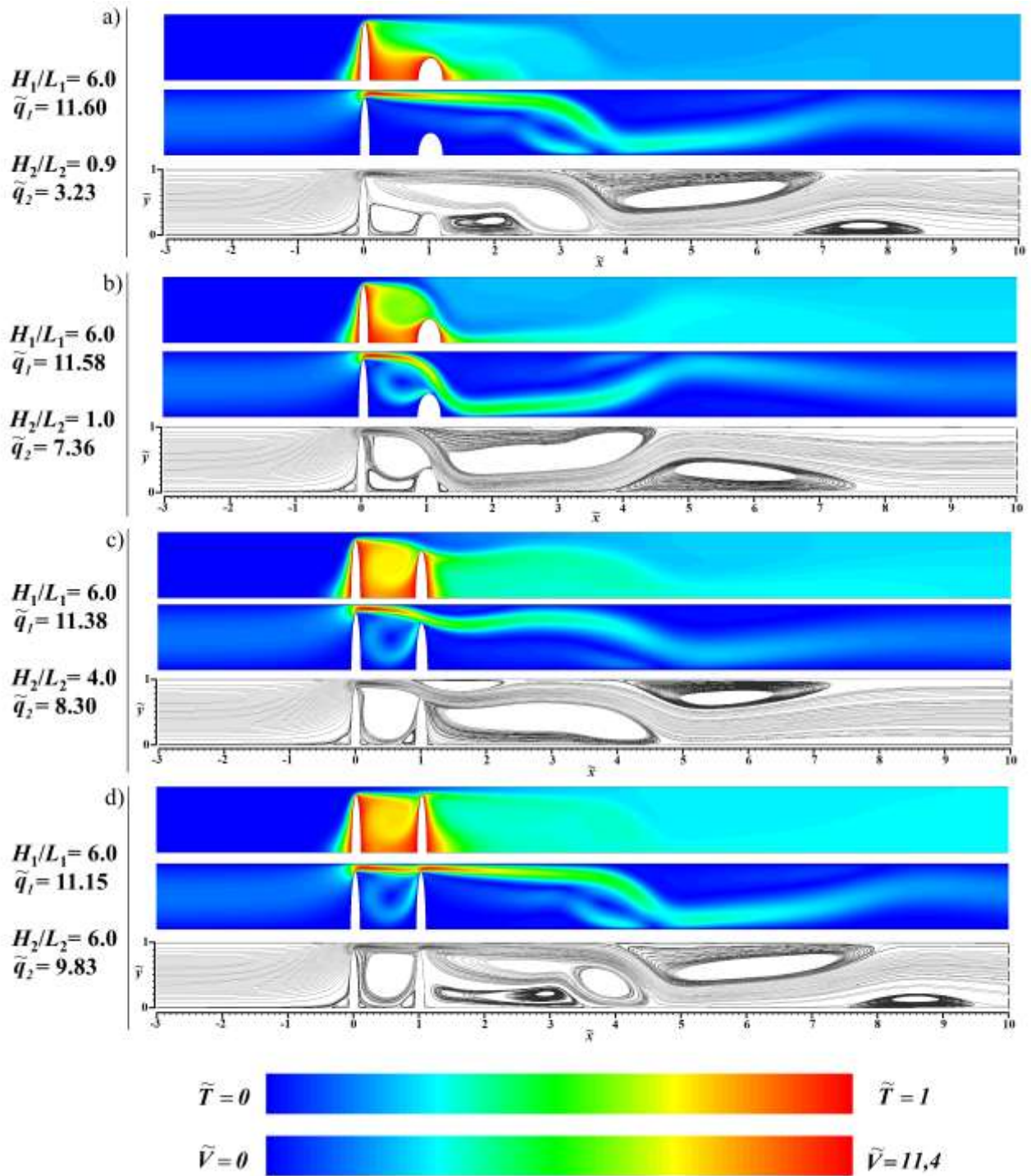
Figure 11 – Temperature, speed and current line topologies considering $Re_H = 100$ for: (a) $H_1/L_1 = 6.0$ and $H_2/L_2 = 0.9$; (b) $H_1/L_1 = 6.0$ and $H_2/L_2 = 1.0$; (c) $H_1/L_1 = 6.0$ and $H_2/L_2 = 4.0$; (d) $H_1/L_1 = 6.0$ and $H_2/L_2 = 6.0$.
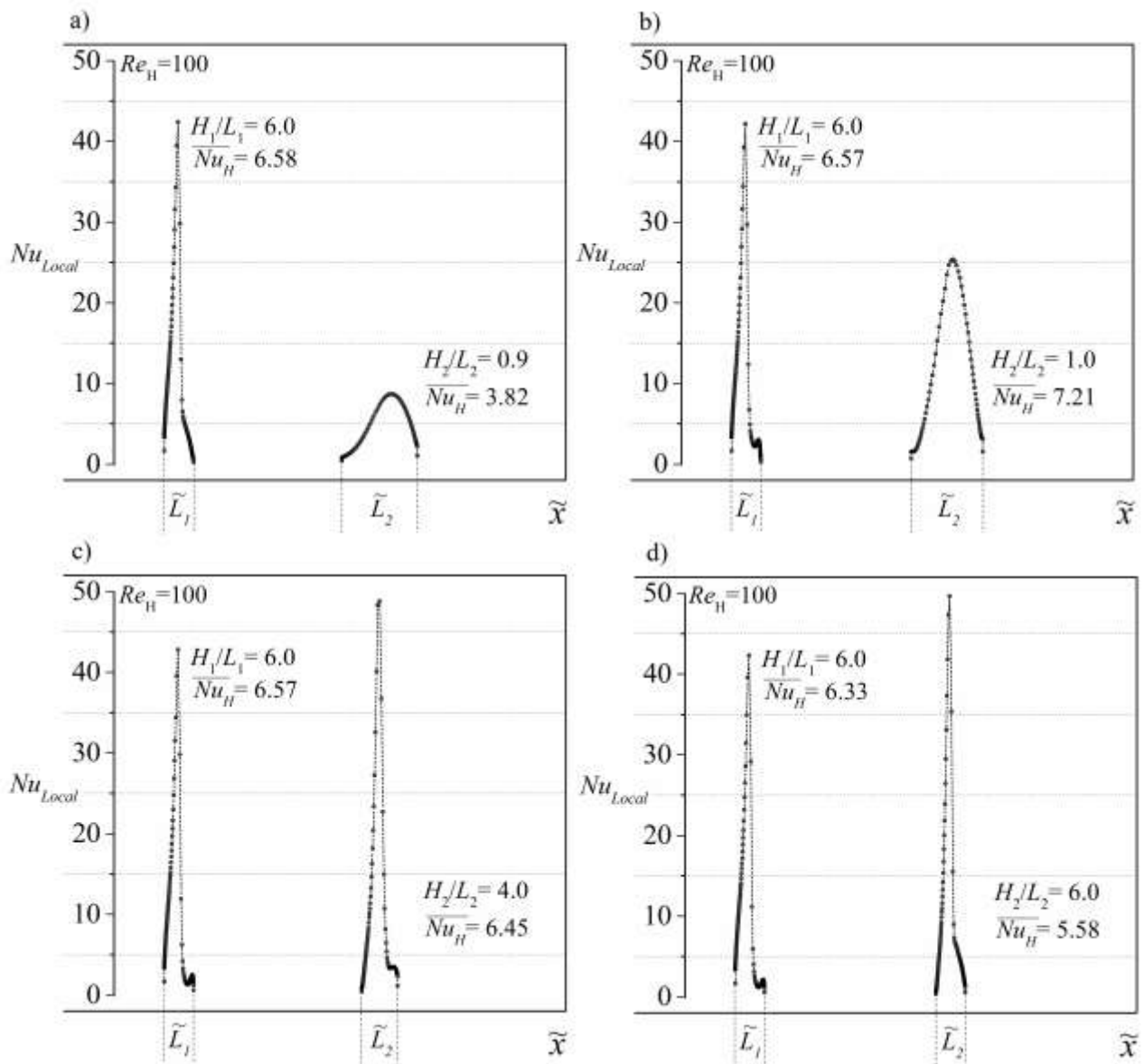
Figure 12 – Effects of the local heat transfer (Nu_{Local}) on the surfaces of blocks 1 and 2 for the geometric configurations given by: (a) $H_1/L_1 = 6.0$ and $H_2/L_2 = 0.9$; (b) $H_1/L_1 = 6.0$ and $H_2/L_2 = 1.0$; (c) $H_1/L_1 = 6.0$ and $H_2/L_2 = 4.0$; (d) $H_1/L_1 = 6.0$ and $H_2/L_2 = 6.0$.
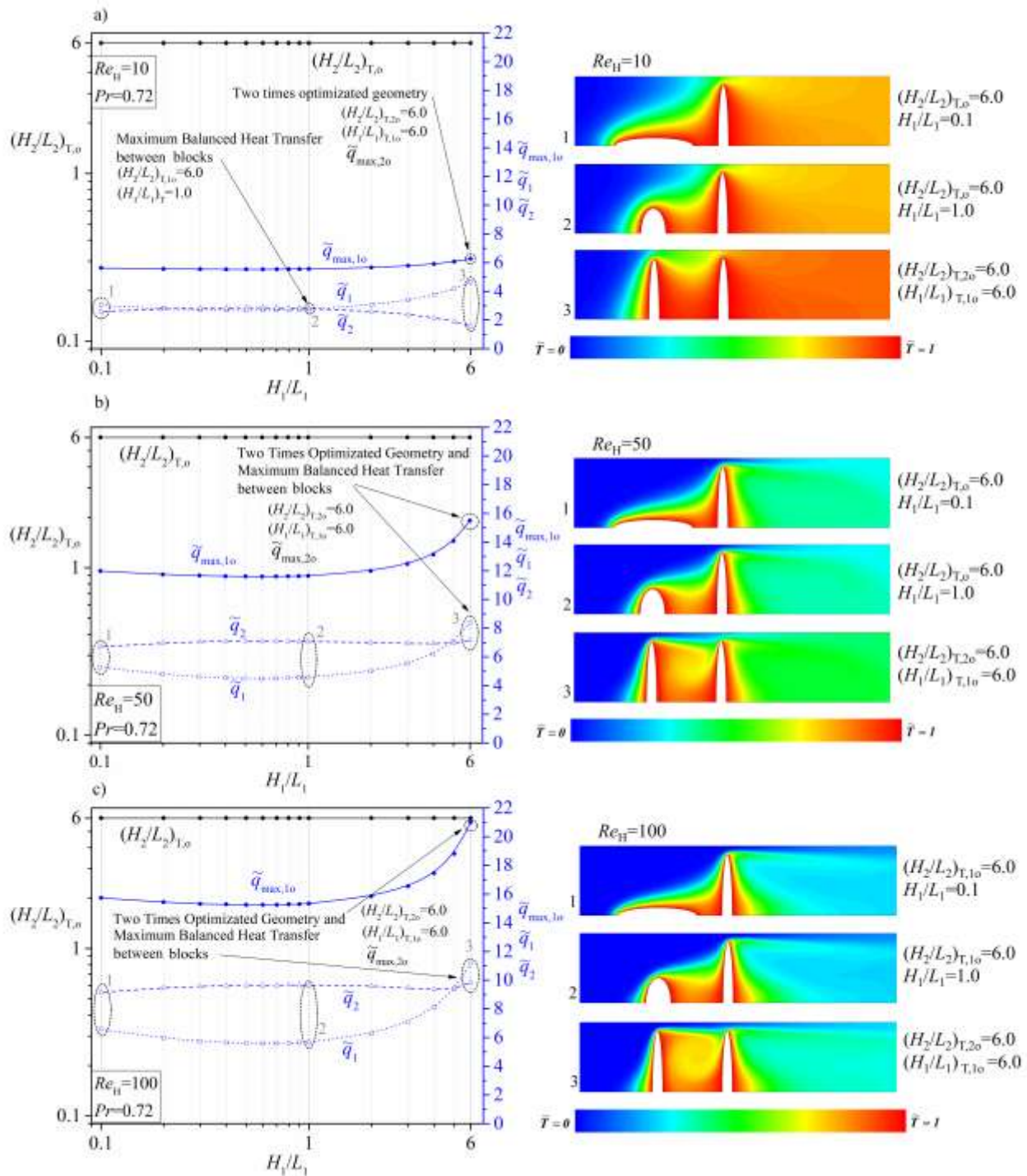
Figure 13 – Optimum performance geometries $(H_2/L_2)_{T,1o}$ and dimensionless heat transfer rates, $\tilde{q}$, $\tilde{q}_1$ e $\tilde{q}_2$ obtained in a first level of optimization as a function of H_1/L_1 for: (a) $Re_H = 10$; (b) $Re_H = 50$; (c) $Re_H = 100$.

50
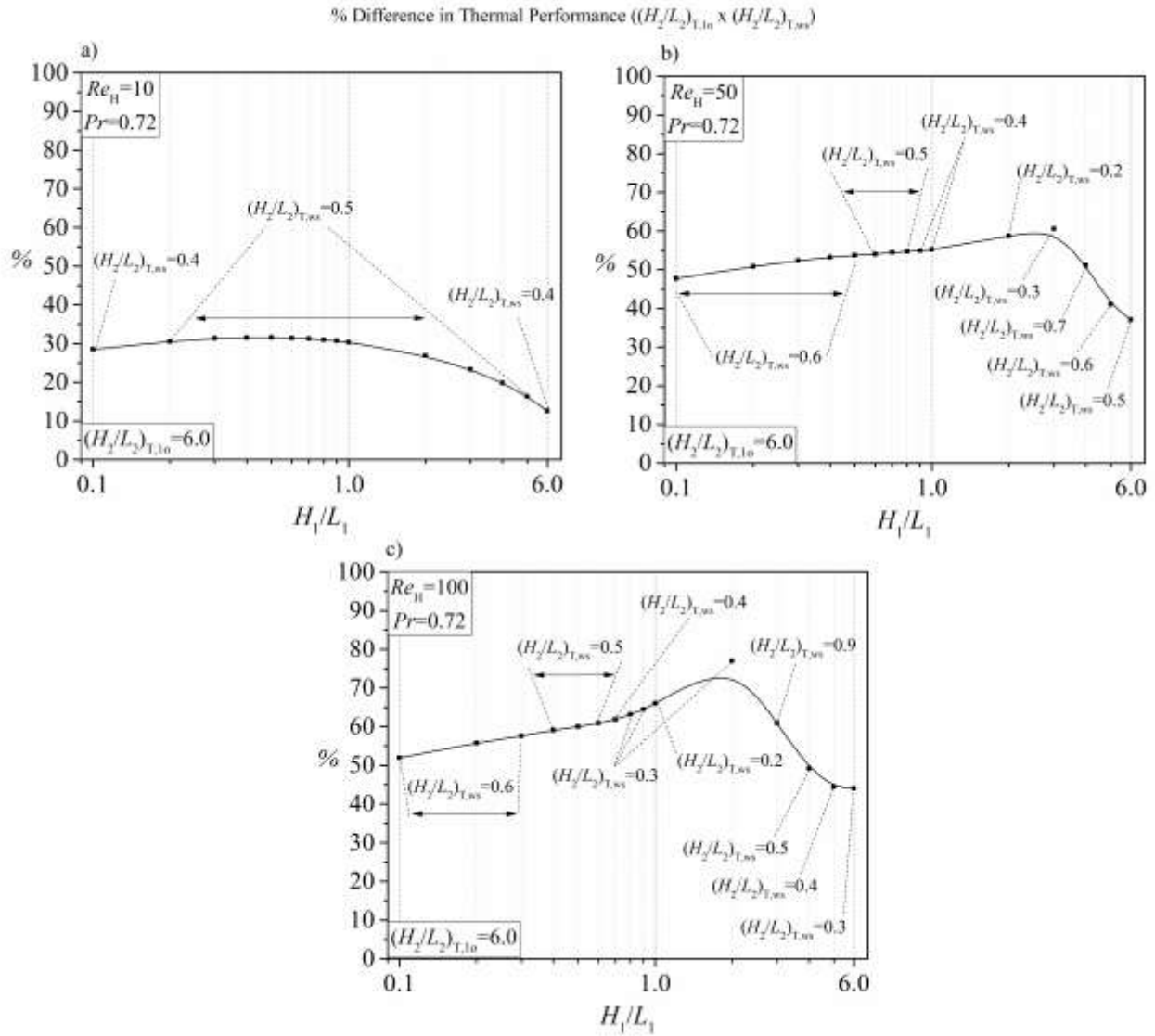
Figure 14 – Percentage difference in thermal performance ($\tilde{q}$) of the once optimized geometries $((H_2/L_2)_{T,1o})$ in relation to lower performance geometries $((H_2/L_2)_{T,ws})$ in a first optimization level, as a function of H_1/L_1, for: (a) $Re_H = 10$; (b) $Re_H = 50$; (c) $Re_H = 100$.
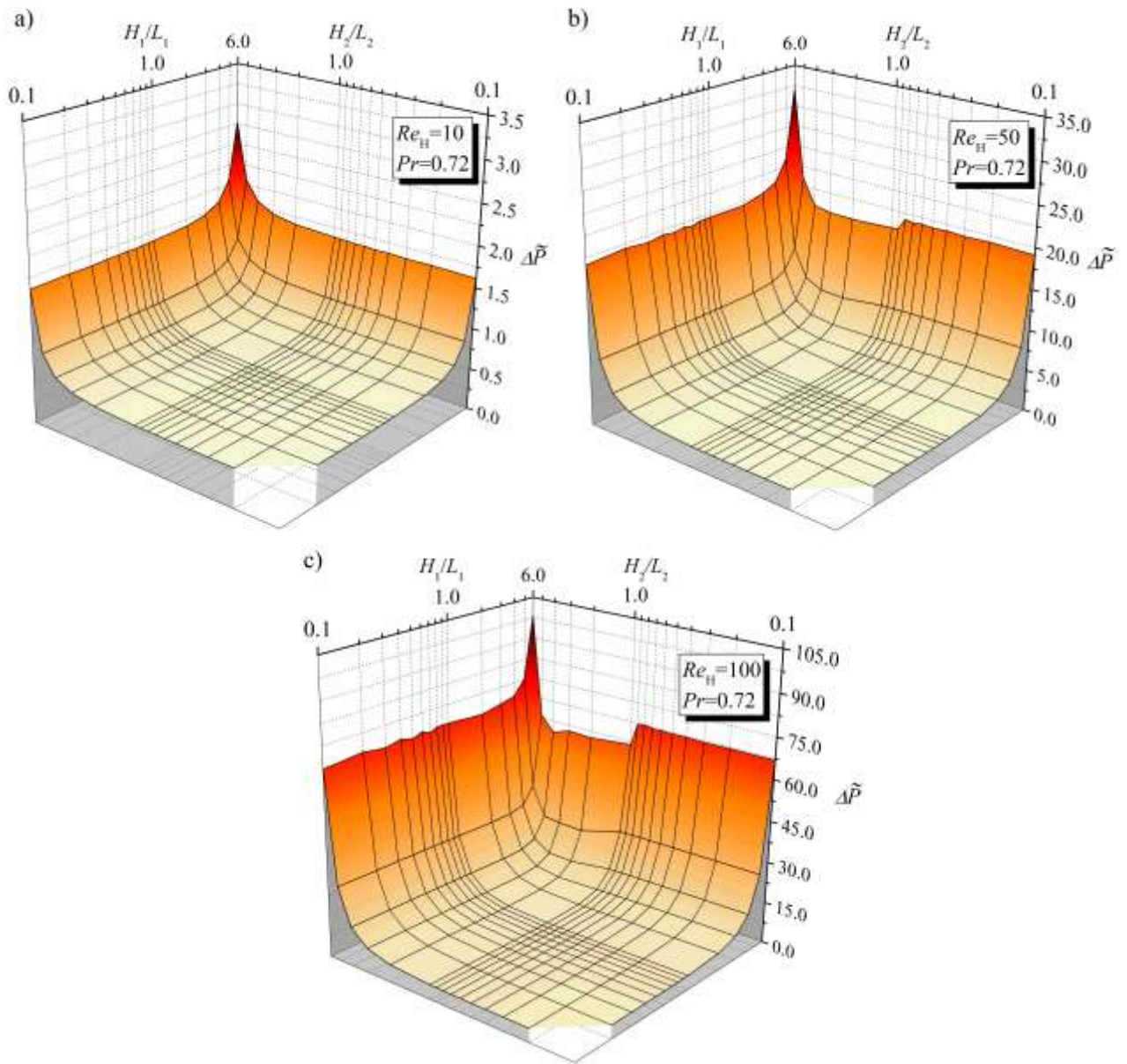
Figure 15 – Study of the pressure drop inside the domain (ΔP) as a function of the degrees of freedom H_1/L_1 and H_2/L_2 for different Reynolds numbers: (a) $Re_H = 10$; (b) $Re_H = 50$; (c) $Re_H = 100$.
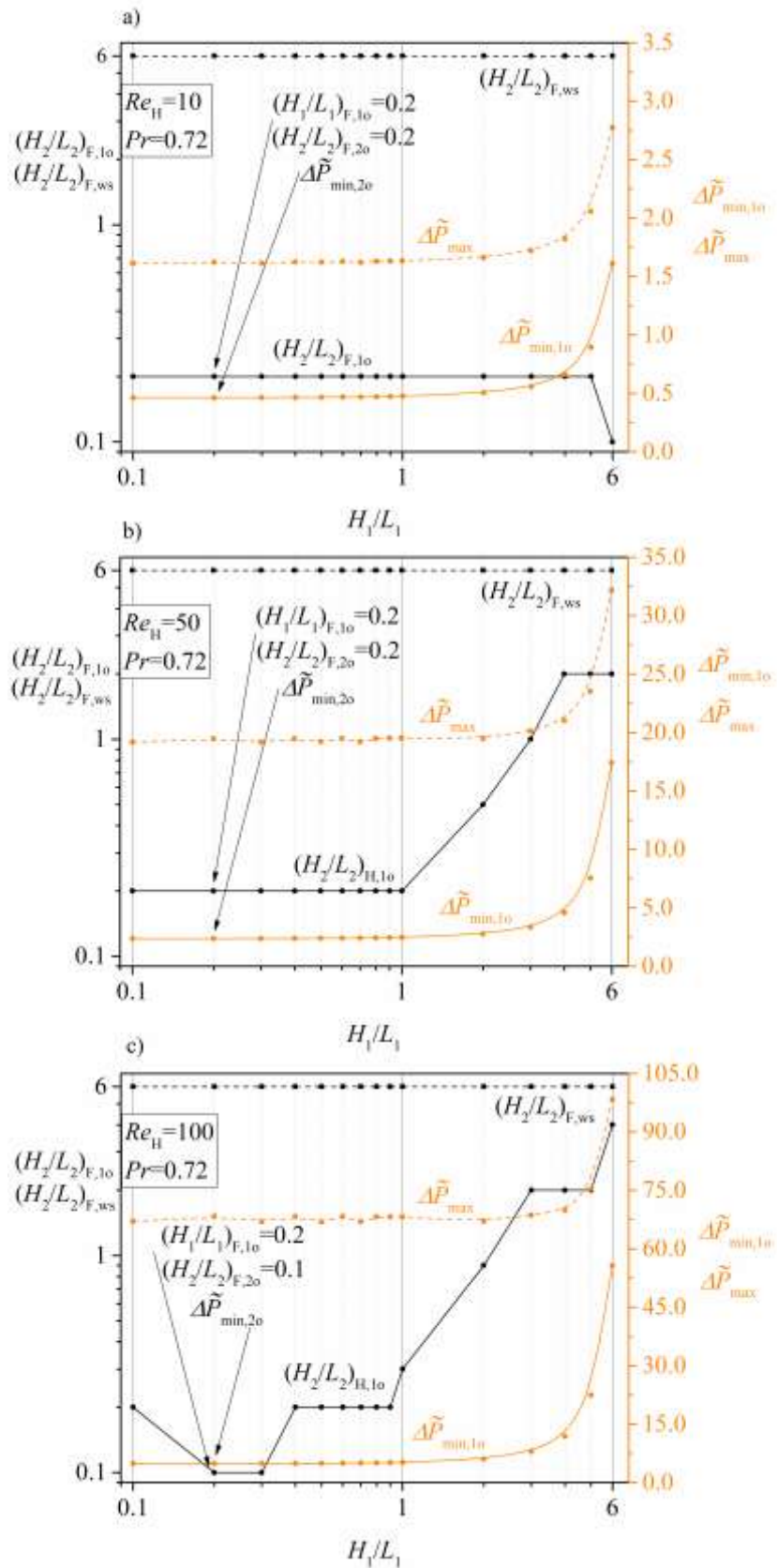
Figure 16 – Optimum and worst performance geometries ((H_2/L_2)$_{F,1o}$ and (H_2/L_2)$_{F,ws}$) and their respective fluid dynamic performances ($\Delta P_{min,1,o}$ and ΔP_{max}) obtained in a first optimization level in function of H_1/L_1 for: (a) $Re_H = 10$; (b) $Re_H = 50$; (c) $Re_H = 100$.
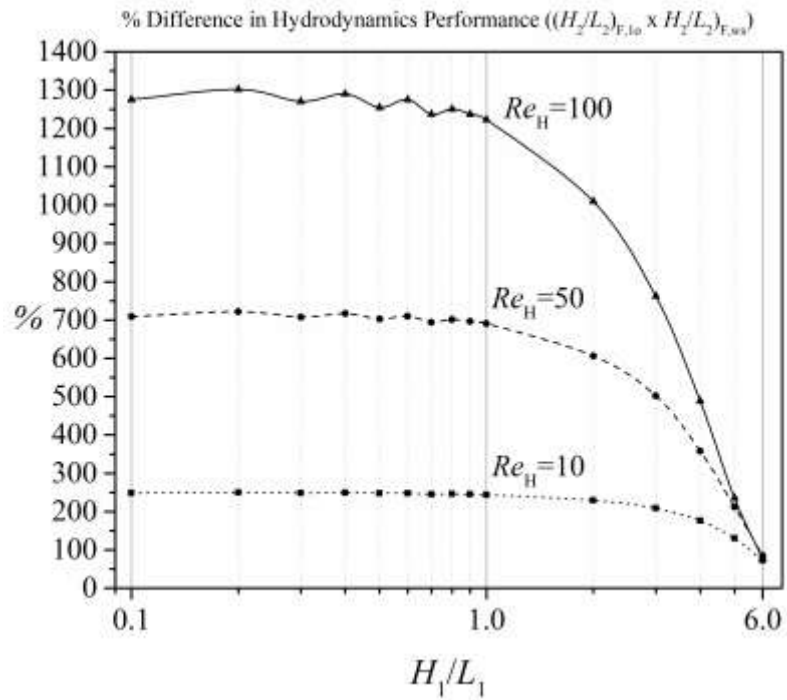
53

% Difference in Hydrodynamics Performance $((H_2/L_2)_{F,1o} \times H_2/L_2)_{F,ws})$

Figure 17 – Percentage difference in the fluid dynamics performance of the once optimized geometries $((H_2/L_2)_{F,1o})$ in relation to the lower performance geometries $((H_2/L_2)_{F,ws})$ in a first optimization level, as a function of H_1/L_1, for: (a) $Re_H = 10$; (b) $Re_H = 50$; (c) $Re_H = 100$.
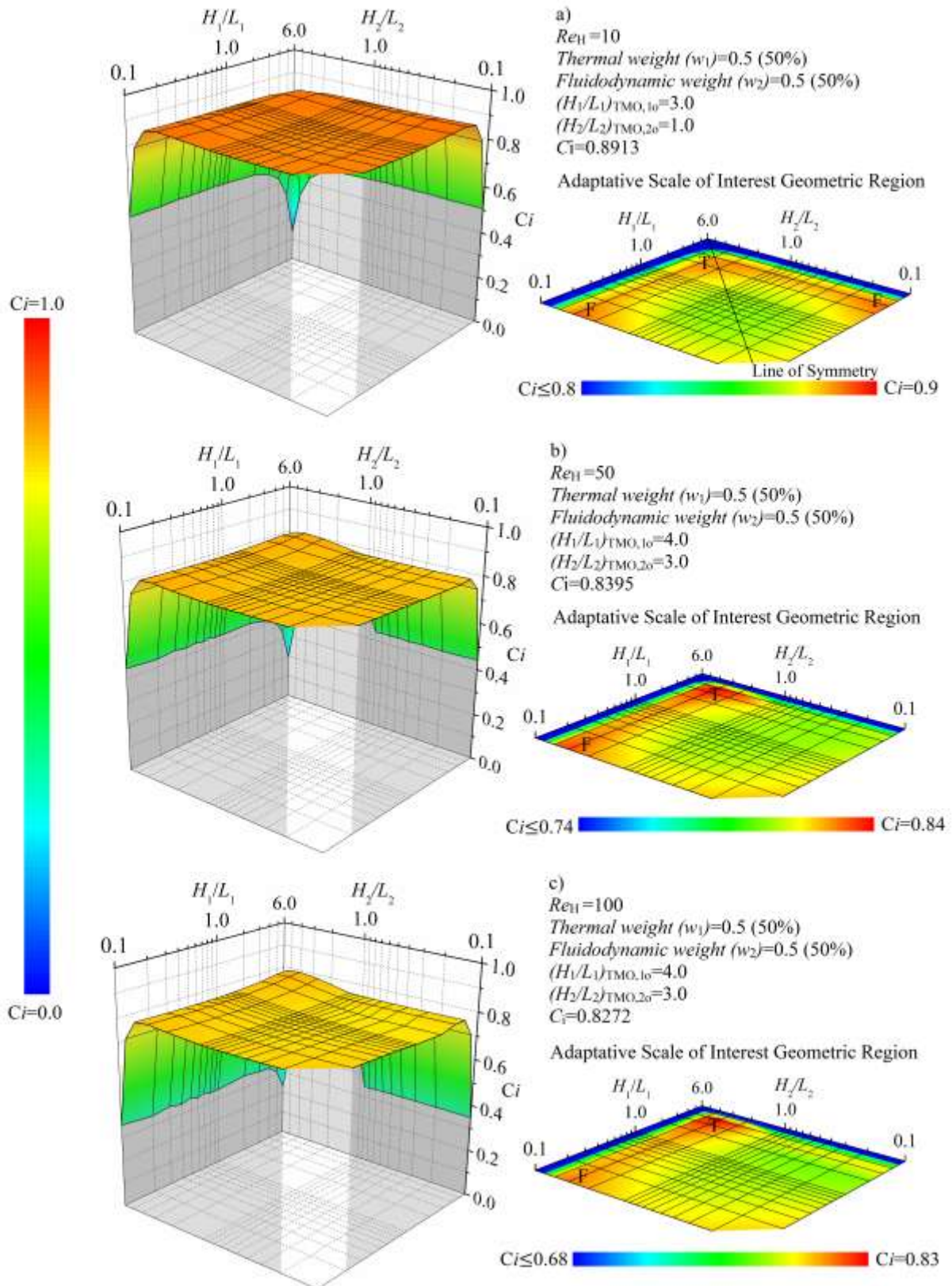
Figure 18 – Response surface referring to the multi-objective performance indicator (C_i) as a function of H_1/L_1 and H_2/L_2 for: (a) $Re_H = 10$; (b) $Re_H = 50$; (c) $Re_H = 100$, calculated by means of the TOPSIS method.
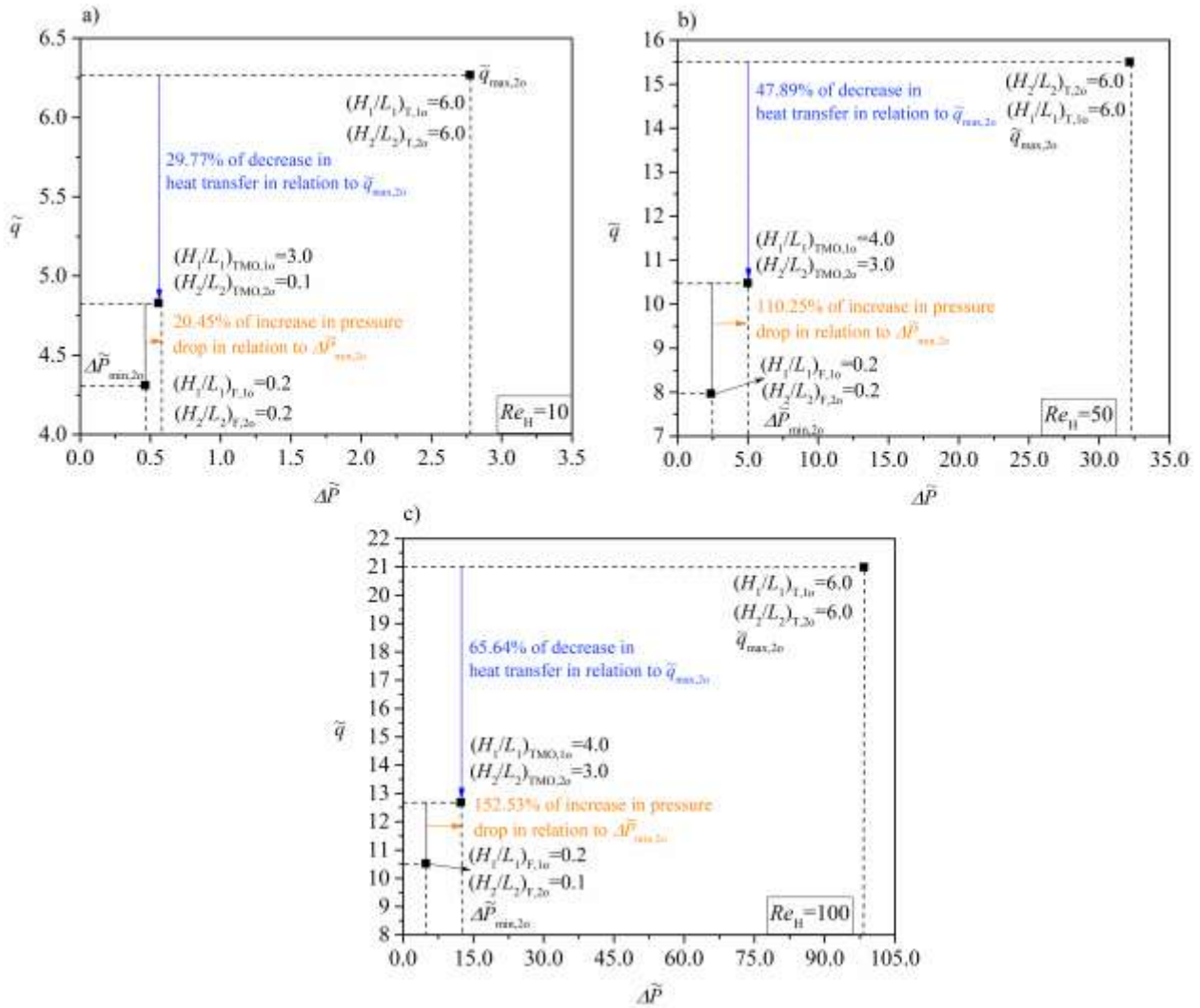
Figure 19 – Comparison between the optimal geometries for the thermal objective $((H_2/L_2)_{T,1o}$, $(H_2/L_2)_{T,2o})$, the fluid dynamic objective $((H_2/L_2)_{F,1o}$ and $(H_2/L_2)_{F,2o})$ and the multi-objective $((H_2/L_2)_{TMO,1o}$ and $(H_2/L_2)_{TMO,2o})$ for: (a) $Re_H = 10$; (b) $Re_H = 50$; (c) $Re_H = 100$, as a function of $\tilde{q}$ and ΔP.
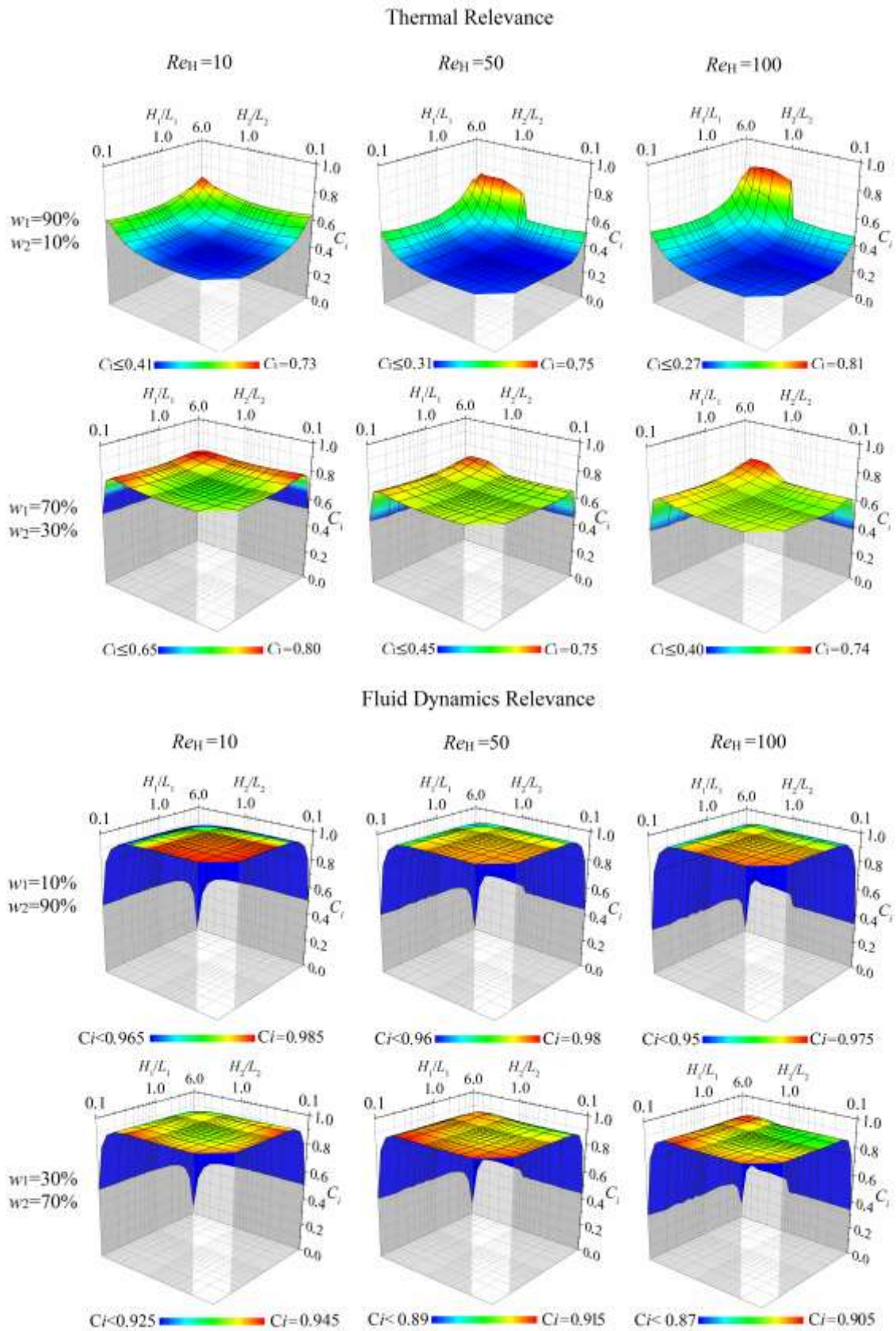
Figure 20 – Multi-objective performance surfaces (C_i), considering different relevance of the thermal and fluid dynamic purposes (w_1 and w_2).